

The BFKL Pomeron in Deep Inelastic Diffractive Dissociation near $t = 0$

J. Bartels, H.Lotter and M.Wüsthoff

II. Institut für Theoretische Physik, Universität Hamburg

Abstract: The small- t behaviour of the deep inelastic diffractive dissociation cross section in the triple Regge region is investigated, using the BFKL approximation in perturbative QCD. We show that the cross section is finite at $t = 0$, but the diffusion in $\ln k_t^2$ leads to a large contribution of small momenta at the triple Pomeron vertex. We study the dependence upon the total energy and the invariant mass. At $t = 0$, there is a decoupling of the three BFKL singularities which is a consequence of the conservation of the conformal dimension. For large invariant masses, the four gluon state in the upper t-channel plays an important role and cannot be neglected.

1 Introduction

The study of perturbative QCD in the triple-Regge limit has recently attracted some interest [1, 2]. If one interpretes the observed strong rise of F_2 at small x as a signal for the BFKL-Pomeron [3], it is natural to ask for corrections to this new piece of perturbative QCD, and an obvious place to look for such terms is the triple Regge limit. There may also be some interest in this limit from an experimental point of view: some of the observed “rapidity gap events” [4, 5] may belong to a kinematical region where perturbative QCD is applicable.

In [2] an attempt has been made to derive an analytic formula for the triple Regge inclusive cross section which lies at the same level of accuracy as the BFKL Pomeron. The result was given in a somewhat abstract form, and, so far, only a few rather general properties have been studied. The general structure of the cross section formula is illustrated in Fig.1a: starting from the top, the fermion box first couples to a BFKL-ladder. At the transition: two gluons \rightarrow four gluons a new vertex function appears. Below this vertex the four-gluon state starts where the gluons interact pairwise in all possible ways. Finally, the four-gluon state branches into the two BFKL ladders at the bottom. In addition to this general structure, there is also a contribution where the upper BFKL-ladder couples directly to the lower ones (Fig.1b).

Based upon the experience with BFKL Pomeron, we expect that the formalism developed in [2] is suited to study the whole range of momentum transfer t of the diffractive dissociation cross section (provided that $\sqrt{-t}$ is still smaller than M , the missing mass of produced hadronic system). Nevertheless, there are several reasons to believe that the point $t = 0$ plays a very special role and perturbation theory may even not be applicable at all. Firstly, the early hard scattering approach of ref. [6, 7] (and similar calculations later on) has shown that the large transverse momenta at the two gluons \rightarrow four gluons- vertex (fig. 1a) are suppressed like dk_t^2/k_t^4 , i.e. small transverse momenta dominate. Without invoking further corrections, the cross section would diverge at $k_t^2 = 0$: in the framework of the GLR equation which leads to a saturation of the Pomeron it is the unitarity corrections (screening) to the lower Pomerons which provide the necessary suppression at small k_t^2 . Since the saturation begins at a rather large momentum scale ($2 - 4 GeV^2$, depending upon the

ratios M^2/s [7]), this mechanism tends to predict hard final states. Secondly, also within BFKL physics the point $t = 0$ is exceptional: within the lower Pomerons the diffusion in $\ln k_t^2$ extends into both the ultraviolet and the infrared regions, whereas for $t \neq 0$ the diffusion into the infrared region where perturbation theory becomes unreliable is stopped by the momentum scale t . One therefore expects, for the point $t = 0$, the “dangerous” region of small k_t to play a much more important role than for the case $t \neq 0$. This expectation has recently been confirmed by Mueller [1], using the large- N_c approximation. As a result of this approximation, the four gluon state above the triple Pomeron vertex is absent, and one is lead directly to a study of the diagrams shown in Fig.1b. The final result of this study is an explicit formula for the inclusive cross section, showing the dependence upon the energy variables s , M , and the momentum transfer t . The latter one is of particular interest: for an intermediate t -region, the cross section goes as $1/\sqrt{-t}$. This behaviour hints at some sort of singular behaviour at $t = 0$, in agreement with what one might expect in the diffusion picture. From this study, however, it is not clear what happens at $t = 0$, in particular, whether the whole perturbative analysis breaks down or not.

The more general reason why, from the theoretical point of view, it is important to understand the small- t behaviour of the diffractive dissociation cross section is the problem of unitarization. It is well-known that the sum of the leading logarithms at sufficiently large energies (or sufficiently small x_{Bj}) runs into conflict with unitarity, and the way in which unitarity is restored is still an open question. Diffractive dissociation is not contained in the leading logarithmic approximation and, therefore, represents a (observable) correction which contributes to the unitarization procedure. Within the GLR-equation, the finite limit of the cross section at $t = 0$ requires the complete unitarization (saturation) of the lower Pomerons. Similarly, in [12] it was shown that, while single unitarity corrections have large infrared contributions, their resummation leads to strong cancellations. In both cases, one expects the final state to be rather hard. The process of diffractive dissociation may therefore become a very sensitive tool in exploring the unitarization mechanism. For example, one might count the number of events in dependence on a lower cutoff on k_t of the final state or, alternatively, measure the momentum transfer t . At which scale the saturation

occurs is still an open question, since the GLR-equation is only a crude estimation compared to a complete procedure of unitarization. The HERA data will soon show, whether a value for k_t^2 of about $2 - 4 \text{ GeV}^2$ is justified.

In this paper, we are going to investigate the small t -region of the cross section formula of [2], in particular the point $t = 0$. As one of the main results of this paper we will show that the BFKL approach to the diffractive dissociation, in spite of the dk_t^2/k_t^4 -behaviour at large k_t , is infrared safe, and the limit $t = 0$ exists. At the same time, however, the BFKL diffusion has entered into the infrared region and thus emphasizes the need to include unitarizing corrections to the leading logarithmic approximation. We believe that this observation is important from the point of view of theoretical consistency: it shows that, within the BFKL approach, a smooth transition from a finite t down to $t = 0$ is possible without running into infrared singularities. Consequently, the approximation used in [2] represents a well-defined starting point for approaching the unitarization problem. Whether the (leading logarithmic) formula of [2] can already be used for deducing experimental signatures remains less clear. It is encouraging that a rough estimate of the ratio of diffractive events over all DIS-events gives a reasonable value. Furthermore, HERA-data, so far, seem to support the dominance [9] of events with low k_t : this is in qualitative agreement with the strong diffusion into the infrared region. Therefore, it seems worthwhile to study the dynamics of the unscreened BFKL-Pomeron in more detail, even before addressing the question of unitarization. Certain characteristics may very well survive the unitarization procedure, and it is important to check whether they may serve as signals to support or rule out the BFKL-dynamics.

Apart from the result that the BFKL cross section formula has a finite limit at $t = 0$ our analysis contains a detailed saddle point analysis and investigates, as a function of t near $t = 0$, the dependence upon s , M^2 , and Q^2 . For $|t|$ of the order of Q^2 , our analysis confirms the $1/\sqrt{-t}$ behaviour found in [12] in the large- N_c - approximation. Moving towards smaller t -values, the shape of the t -distribution changes, and the cross section reaches, at $t = 0$, a finite limit. At the same time, the derivative with respect to t tends to infinity. For small t one observes a shrinkage, i.e. the cusp becomes narrower as $s \rightarrow \infty$ (the typical width shrinks with some inverse power of s/M^2). All

these changes as a function of t are accompanied by a very peculiar dependence upon s and M^2 . In particular, at $t = 0$ one observes a decoupling of the lower BFKL Pomerons from the BFKL singularity above. Much of this striking behaviour can be traced back to the conformal invariance of the BFKL approximation: at $t = 0$ we find a conservation law of the conformal dimension of the BFKL ladders above and below the triple Pomeron vertex.

Our paper will be organized as follows. We begin with the simplest case, the diffractive production of a $q\bar{q}$ -pair in the triple Regge region near $t = 0$. This simple case already shows the main result, namely the conservation law of conformal dimensions and its implication for the high energy behavior. The advantage of first presenting this simpler case lies in the fact that we are able to present an analytic expression for the M^2 -integrated cross section which can directly be used for a comparison with observed event rates. The discussion will first be done in momentum space; in the subsequent section we repeat the derivation in coordinate space where a more intuitive picture has been developed [12, 13]. The generalization to the production of $q\bar{q}$ + gluons will be described in Section 4; since the analysis presented in this part will be rather technical, we shall give a short summary at the end of this section. In the final section we discuss a few implications of the results of this paper.

2 Diffractive Production of $q\bar{q}$ -Pairs Near $t = 0$

We begin with the M^2 -integrated cross section for the process (Fig.2a) $\gamma^* + \text{proton} \rightarrow (q\bar{q}) + \text{proton}$, where M is the invariant mass of the quark pair, t the square of the momentum transferred from the proton to the quark pair, and $1/x_B = s/Q^2$ the total energy. We are interested in the limit of small x_B and keep t as a small variable parameter.

Following the notation of [2] we use the integral representation

$$\frac{d\sigma}{dt} = \sum_f e_f^2 \frac{\alpha_{em}(2\pi)^3}{8\pi Q^4} \int \frac{d\omega_1}{2\pi i} \int \frac{d\omega_2}{2\pi i} \left(\frac{1}{x_B} \right)^{\omega_1 + \omega_2} F(\omega_1, \omega_2, t), \quad (2.1)$$

where the partial wave consists of the three building blocks illustrated in Fig.2b : at the upper end we have the four-gluon amplitude $D_{(4;0)}^{(1;++)}$, below the two BFKL Pomerons, and at the bottom we use a form factor for the coupling of the BFKL ladders to the proton. The four-gluon amplitude

has been studied in [2]. It can be rewritten as a sum of two-gluon amplitudes:

$$\begin{aligned}
D_{(4,0)}^{(1;+,+)}(\mathbf{k}_1, \mathbf{k}_2, \mathbf{k}_3, \mathbf{k}_4) &= g^2 \frac{\sqrt{2}}{3} \cdot \\
&\left\{ D_{(2;0)}(\mathbf{k}_1, \mathbf{k}_2 + \mathbf{k}_3 + \mathbf{k}_4) + D_{(2;0)}(\mathbf{k}_2, \mathbf{k}_1 + \mathbf{k}_3 + \mathbf{k}_4) \right. \\
&+ D_{(2;0)}(\mathbf{k}_3, \mathbf{k}_1 + \mathbf{k}_2 + \mathbf{k}_4) + D_{(2;0)}(\mathbf{k}_4, \mathbf{k}_1 + \mathbf{k}_2 + \mathbf{k}_3) \\
&\left. - D_{(2;0)}(\mathbf{k}_1 + \mathbf{k}_2, \mathbf{k}_3 + \mathbf{k}_4) - D_{(2;0)}(\mathbf{k}_1 + \mathbf{k}_3, \mathbf{k}_2 + \mathbf{k}_4) - D_{(2;0)}(\mathbf{k}_1 + \mathbf{k}_4, \mathbf{k}_2 + \mathbf{k}_3) \right\} .
\end{aligned} \tag{2.2}$$

For $D_{(2;0)}(\mathbf{k}, -\mathbf{k})$ it is convenient to use a Mellin transform with respect to the variable k^2/Q^2 :

$$D_{(2;0)}(k^2) = \int \frac{d\mu}{2\pi i} \left(\frac{k^2}{Q^2} \right)^{-\mu} \tilde{D}_{(2;0)}(\mu), \tag{2.3}$$

where the μ -contour runs along the imaginary axis, intersecting the real axis within the interval $(-1, 0)$ (in the following we shall use, as the intersection with the real axis, the point $-1/2$; we shall then use the notation $\mu = -1/2 - i\nu$). The function $\tilde{D}_{(2;0)}(\mu)$ has poles at positive and negative integers, and a detailed discussion is contained in [2]. In this paper we only need the behaviour near $\mu = -1$

$$\tilde{D}_{(2;0)} \approx \sum_f \frac{e_f^2 \alpha_s \sqrt{8}}{2\pi} \frac{4}{3} \frac{1}{(\mu + 1)^2} \tag{2.4}$$

and near $\mu = -\frac{1}{2}$:

$$\tilde{D}_{(2;0)} \approx \sum_f \frac{e_f^2 \alpha_s 9\sqrt{2}\pi^2}{16} \tag{2.5}$$

Next we turn to the BFKL Pomeron. Since we want to study the t -dependence for $t \neq 0$ we need an expression for the BFKL-pomeron for non-zero momentum transfer. The BFKL-pomeron is determined by a Bethe-Salpeter type of equation in two dimensional transverse space. Lipatov [14] has shown that the configuration space representation of this equation is invariant under two dimensional conformal transformations. Due to this symmetry it can be diagonalized by a conformal partial wave expansion. Using orthonormality and completeness of the conformal partial waves Lipatov found an analytic expression for the sum of the nonforward ladders. By a straightforward

Fourier transformation, this expression leads to the following momentum representation ¹:

$$\Phi_\omega(\mathbf{k}, \mathbf{k}', \mathbf{q}) = \int_{-\infty}^{+\infty} \frac{d\nu}{2\pi} \frac{1}{\omega - \chi(0, \nu)} E^{(\nu)}(\mathbf{k}, \mathbf{q} - \mathbf{k}) E^{(\nu)*}(\mathbf{k}', \mathbf{q} - \mathbf{k}') \quad (2.6)$$

where we have restricted ourselves to zero conformal spin. The eigenvalues $\chi(0, \nu)$ of the BFKL-kernel are given by:

$$\chi(0, \nu) = \frac{g^2 N_c}{4\pi^2} [2\psi(1) - \psi(\frac{1}{2} + i\nu) - \psi(\frac{1}{2} - i\nu)] \quad (2.7)$$

The conformal partial waves have the momentum representation

$$\begin{aligned} E^{(\nu)}(\mathbf{k}, \mathbf{q} - \mathbf{k}) &= \frac{4^{-i\nu}}{4\pi} \frac{\Gamma(1 + 2i\nu)}{\Gamma(-2i\nu)} \frac{\Gamma(-\frac{1}{2} - i\nu)}{\Gamma(\frac{3}{2} + i\nu)} \frac{\Gamma^2(\frac{1}{2} - i\nu)}{\Gamma^2(\frac{1}{2} + i\nu)} \int d^2\rho_1 d^2\rho_2 e^{i\mathbf{k}\rho_1 + i(\mathbf{q}-\mathbf{k})\rho_2} \left(\frac{\rho_{12}^2}{\rho_1^2 \rho_2^2}\right)^{\frac{1}{2} - i\nu} \\ &= 2\pi \frac{\Gamma(1 + 2i\nu)}{\Gamma(-2i\nu)} \frac{\Gamma(-\frac{1}{2} - i\nu)}{\Gamma(\frac{1}{2} + i\nu)} \frac{\Gamma(\frac{3}{2} - i\nu)}{\Gamma(\frac{1}{2} + i\nu)} \\ &\quad \cdot \int_0^1 dx [x(1-x)]^{-\frac{1}{2} + i\nu} [\mathbf{q}^2 x(1-x) + (\mathbf{k} - x\mathbf{q})^2]^{-\frac{3}{2} - i\nu} \\ &\quad \cdot {}_2F_1\left(\frac{3}{2} + i\nu, i\nu - \frac{1}{2}, 1; \frac{(\mathbf{k} - x\mathbf{q})^2}{\mathbf{q}^2 x(1-x) + (\mathbf{k} - x\mathbf{q})^2}\right) \end{aligned} \quad (2.8)$$

The normalization was chosen in such a way ² that in the limit $\mathbf{q} = 0$ the expression (2.6) coincides with the familiar BFKL-Pomeron in the forward direction:

$$\Phi_\omega(\mathbf{k}, \mathbf{k}', \mathbf{q} = 0) = 2(2\pi)^2 \int_{-\infty}^{+\infty} \frac{d\nu}{2\pi} \frac{1}{\omega - \chi(0, \nu)} (\mathbf{k}^2)^{-\frac{3}{2} - i\nu} (\mathbf{k}'^2)^{-\frac{3}{2} + i\nu} \quad (2.9)$$

In (2.8) one has to be careful in taking the limit $q \rightarrow 0$, namely making use of the well known properties of the hypergeometric functions one finds

$$E^{(\nu)}(\mathbf{k}, \mathbf{q} \rightarrow 0) = 2\pi[(k^2)^{-3/2 - i\nu} + C(\nu)(k^2)^{-3/2 + i\nu}(q^2)^{-2i\nu}] \quad (2.10)$$

where $C(\nu)$ is analytic in the range $-1/2 < \text{Im}(\nu) < 1/2$ and has the property $C(-\nu) = 1/C(\nu)$. Hence, $E^{(\nu)}$ remains finite at $\mathbf{q} = 0$ only if $\text{Im}(\nu) > 0$. If $\text{Im}(\nu) < 0$, $E^{(\nu)}$ becomes infinite. For $E^{(\nu)*}$ the converse is true. So, one of the two factors, $E^{(\nu)}$ or $E^{(\nu)*}$, becomes infinite, no matter what value of ν we choose. However, in (2.6) only the product of the two $E^{(\nu)}$ -functions appears: $E^{(\nu)}(\mathbf{k}, \mathbf{q} \rightarrow 0) E^{(\nu)*}(\mathbf{k}', \mathbf{q} \rightarrow 0) = (2\pi)^2[(\mathbf{k}^2)^{-3/2 - i\nu} (\mathbf{k}'^2)^{-3/2 + i\nu} + (\mathbf{k}^2)^{-3/2 + i\nu} (\mathbf{k}'^2)^{-3/2 - i\nu} +$

¹Our normalization differs from Lipatov's one by factors of 2π which are included in the integration measure in momentum space

²It differs from Lipatov's functions by some Γ factors.

$C(\nu)^2(\mathbf{k}^2)^{-3/2-i\nu}(\mathbf{k}'^2)^{-3/2-i\nu}(q^2)^{2i\nu} + 1/C(\nu)^2(\mathbf{k}^2)^{-3/2+i\nu}(\mathbf{k}'^2)^{-3/2+i\nu}(q^2)^{-2i\nu}$. In the third and the fourth term, using the variable $\mu = -1/2 - i\nu$, we have to shift the contour of integration to the left and to the right, respectively. Since $C(\nu)$ is analytic, both terms vanish. In the second term we change from ν to $-\nu$. As a result we have $\int d\nu E^{(\nu)}(\mathbf{k}, \mathbf{q} \rightarrow 0)E^{(\nu)*}(\mathbf{k}', \mathbf{q} \rightarrow 0) = 2(2\pi)^2 \int d\nu (\mathbf{k}^2)^{-3/2-i\nu}(\mathbf{k}'^2)^{-3/2+i\nu}$, i. e. we get the right answer, if we simply write $E^{(\nu)}(\mathbf{k}, \mathbf{q} \rightarrow 0) = \sqrt{2} 2\pi (k^2)^{-3/2-i\nu}$. In the following, whenever we take the limit $\mathbf{q} \rightarrow 0$, we shall use this effective prescription.

We mention a few properties of (2.8). For $\mathbf{q} \neq 0$, the limit $\mathbf{k} \rightarrow 0$ is singular [15]. By explicit calculation one finds:

$$E^{(\nu)}(\mathbf{k}, \mathbf{q} - \mathbf{k}) = 2\pi\delta^{(2)}(\mathbf{k}) \left(\frac{1}{q^2}\right)^{\frac{1}{2}+i\nu} \frac{\Gamma(1+2i\nu)}{\Gamma(-2i\nu)} \frac{\Gamma(-\frac{1}{2}-i\nu)\Gamma(\frac{1}{2}-i\nu)}{\Gamma(\frac{3}{2}+i\nu)\Gamma(\frac{1}{2}+i\nu)} + O\left(\frac{\mathbf{q} \cdot \mathbf{k}}{\mathbf{k}^2}\right) \quad (2.11)$$

The delta-function term is dictated by the conformal invariance of the BFKL-kernel, and it does not contribute if the BFKL-Pomeron is coupled to an external color singlet state which vanishes as $\mathbf{k} \rightarrow 0$ (or $\mathbf{q} - \mathbf{k} \rightarrow 0$). A useful regularization of the $\mathbf{k} = 0$ - limit is obtained if in (2.8) we introduce a nonzero conformal dimension λ for the (reggeized) gluon field [16] :

$$\begin{aligned} E^{(\nu,\lambda)}(\mathbf{k}, \mathbf{q} - \mathbf{k}) &= \frac{4^{-i\nu}}{2\pi} \frac{\Gamma(1+2i\nu)}{\Gamma(-2i\nu)} \frac{\Gamma(-\frac{1}{2}-i\nu)}{\Gamma(\frac{3}{2}+i\nu)} \frac{\Gamma^2(\frac{1}{2}-i\nu)}{\Gamma^2(\frac{1}{2}+i\nu)} \\ &\cdot \int d^2\rho_1 d^2\rho_2 e^{i\mathbf{k}\rho_1 + i(\mathbf{q}-\mathbf{k})\rho_2} \frac{(\rho_{12}^2)^{\frac{1}{2}-i\nu-\lambda}}{(\rho_1^2)^{\frac{1}{2}-i\nu}(\rho_2^2)^{\frac{1}{2}-i\nu}} \\ &= 4^{1-\lambda}\pi \frac{\Gamma(1+2i\nu)}{\Gamma(-2i\nu)} \frac{\Gamma(-\frac{1}{2}-i\nu)}{\Gamma(\frac{3}{2}+i\nu)} \frac{\Gamma(\frac{3}{2}+i\nu-\lambda)\Gamma(\frac{3}{2}-i\nu-\lambda)}{\Gamma^2(\frac{1}{2}+i\nu)} \\ &\cdot \int_0^1 dx x^{-\frac{1}{2}+i\nu}(1-x)^{-\frac{1}{2}+i\nu} [\mathbf{q}^2 x(1-x) + (\mathbf{k} - x\mathbf{q})^2]^{-\frac{3}{2}+i\nu+\lambda} \\ &\cdot {}_2F_1\left(\frac{3}{2}+i\nu-\lambda, -\frac{1}{2}+i\nu+\lambda, 1; \frac{(\mathbf{k} - x\mathbf{q})^2}{\mathbf{q}^2 x(1-x) + (\mathbf{k} - x\mathbf{q})^2}\right) \end{aligned} \quad (2.12)$$

For small \mathbf{k}^2 , one obtains :

$$\begin{aligned} E^{(\nu,\lambda)}(\mathbf{k}, \mathbf{q} - \mathbf{k}) &= 4^{1-\lambda}\pi \frac{\Gamma(1+2i\nu)}{\Gamma(-2i\nu)} \frac{\Gamma(-\frac{1}{2}-i\nu)}{\Gamma(\frac{3}{2}+i\nu)\Gamma^2(\frac{1}{2}+i\nu)} \Gamma(1+2i\nu)\Gamma(1-2i\nu) \\ &\cdot \left(\frac{1}{\mathbf{q}^2}\right)^{\frac{1}{2}+i\nu} (\mathbf{k}^2)^{-1+\lambda} \left[\frac{i}{2\nu} \frac{\Gamma^2(1-\lambda)}{\Gamma(\frac{3}{2}+i\nu-\lambda)\Gamma(-\frac{1}{2}-i\nu+\lambda)} + \text{c.c.} \right] + O\left(\frac{\mathbf{q}\mathbf{k}}{\mathbf{k}^2}\right) \end{aligned} \quad (2.13)$$

which in the limit $\lambda \rightarrow 0$ leads us to (2.11), provided we identify :

$$\lim_{\lambda \rightarrow 0} 2^{1-2\lambda} \left(\frac{1}{\mathbf{k}^2} \right)^{1-\lambda} \cdot \lambda = \delta^{(2)}(\mathbf{k}) \quad (2.14)$$

Finally, we note from (2.6) that, at fixed ν , the BFKL-pomeron factorizes in momentum space. This property is not present in configuration space where the pomeron is a function of two anharmonic ratios which link together the primed and unprimed coordinates [17]. As a by-product of this calculation, we find the conformal partial waves in a mixed-representation which we give here for later use :

$$\begin{aligned} E^{(\nu)}(\rho_{12}, \mathbf{q}) &= \frac{1}{2} \frac{\Gamma(1+2i\nu)}{\Gamma(-2i\nu)} \frac{\Gamma(-\frac{1}{2}-i\nu)}{\Gamma(\frac{3}{2}+i\nu)} \frac{1}{\Gamma^2(\frac{1}{2}+i\nu)} (\mathbf{q}^2)^{-i\nu} \rho_{12} \\ &\int_0^1 dx [x(1-x)]^{-\frac{1}{2}} e^{-i\mathbf{q} \cdot \rho_{12}(1-x)} K_{-2i\nu}(|\mathbf{q}| |\rho_{12}| \sqrt{x(1-x)}) \end{aligned} \quad (2.15)$$

Finally, for the (nonperturbative) coupling of the BFKL ladders to the proton we use, as a guide for the dependence upon a hadronic scale Q_0^2 , the following simple model (at the point $\mathbf{q} = 0$):

$$V(k^2) = C \frac{k^2}{k^2 + Q_0^2} \quad (2.16)$$

where Q_0^2 denotes a hadronic scale of the order of 1GeV^2 . As to dependence upon t and ν , we shall assume that C is a slowly varying function.

Returning to (2.1) and putting together all these ingredients, we arrive at the following expression for the partial wave F :

$$\begin{aligned} F(\omega_1, \omega_2, t) &= \int \frac{d^2 \mathbf{l}}{(2\pi)^3} \int \frac{d^2 \mathbf{m}}{(2\pi)^3} D_{(4;0)}^{(1;++)}(\mathbf{l}, \mathbf{q} - \mathbf{l}, \mathbf{m}, -\mathbf{m} - \mathbf{q}) \\ &\cdot \int \frac{d^2 \mathbf{l}'}{(2\pi)^3} \Phi_{\omega_1}(\mathbf{l}, \mathbf{q} - \mathbf{l}, \mathbf{l}', \mathbf{q} - \mathbf{l}') V(\mathbf{l}', \mathbf{q} - \mathbf{l}') \\ &\cdot \int \frac{d^2 \mathbf{m}'}{(2\pi)^3} \Phi_{\omega_2}(\mathbf{m}, -\mathbf{q} - \mathbf{m}, \mathbf{m}', -\mathbf{q} - \mathbf{m}') V(\mathbf{m}', -\mathbf{q} - \mathbf{m}') \end{aligned} \quad (2.17)$$

where $-\mathbf{q}^2 = t$ denotes the square of the momentum transfer, and Φ and V are given in (2.6), (2.16), resp..

We now turn to (2.17) and study its dependence upon t , near $t = 0$. We begin with the integrations in \mathbf{l} and \mathbf{m} . For $D_{(4;0)}$ we use (2.3), (2.3), and from the two lower Pomerons we have

the two $E^{(\nu)}$ -functions. This defines the vertex $g_{\mu\mu_1\mu_2}(q^2)$:

$$\int \frac{d^2\mathbf{l}d^2\mathbf{m}}{(2\pi)^6} \left[(\mathbf{l}^2)^{-\mu} + ((\mathbf{l}-\mathbf{q})^2)^{-\mu} + (\mathbf{m}^2)^{-\mu} + ((\mathbf{m}+\mathbf{q})^2)^{-\mu} - (\mathbf{q}^2)^{-\mu} - ((\mathbf{l}+\mathbf{m})^2)^{-\mu} - ((\mathbf{l}-\mathbf{m}-\mathbf{q})^2)^{-\mu} \right] E^{(\nu_1)}(\mathbf{l}, \mathbf{l}-\mathbf{q}) E^{(\nu_2)}(\mathbf{m}, -\mathbf{m}-\mathbf{q}) = \frac{(q^2)^{\mu_1+\mu_2-\mu}}{\mu_1+\mu_2-\mu} g_{\mu\mu_1\mu_2}(q^2) \quad (2.18)$$

where we have used $\mu_i = -\frac{1}{2} - i\nu_i$. In course of performing the integrals over \mathbf{l} and \mathbf{m} one finds that, out of the seven terms on the lhs, the result will come from the last two terms only; the other serve as regulators in either the infrared or the ultraviolet region. Rather than presenting details of the calculations, we shall limit ourselves to a brief description of the major steps. First, for the $E^{(\nu)}$ functions we use the representation (2.8): the hypergeometric functions are written as a power series in their arguments, and we consider term by term. It is convenient to perform the shifts $\mathbf{l} \rightarrow \mathbf{l} - \mathbf{q}z_1$, $\mathbf{m} \rightarrow \mathbf{m} + \mathbf{q}z_2$ where z_1 and z_2 denote the x -parameters of the representation (2.8) for the two BFKL-Pomerons. Now it is not difficult to perform the integration over \mathbf{l} : one ends up with a string of terms consisting of one dimensional finite integrals involving hypergeometric functions and powers. For the remaining integral over \mathbf{m} one observes that convergence in the ultraviolet region holds as long as the condition

$$\mu > \mu_1 + \mu_2 \quad (2.19)$$

is satisfied ($\mu_i = -\frac{1}{2} - i\nu_i$), i.e. the μ integration contour is to the right of $\mu_1 + \mu_2$. In the infrared region, q^2 serves as a regulator. Consequently, the lhs of expression (2.18), in the neighbourhood of $\mu = \mu_1 + \mu_2$, behaves as

$$\frac{(q^2)^{\mu_1+\mu_2-\mu}}{\mu_1+\mu_2-\mu} \cdot g_{\mu\mu_1\mu_2}(q^2), \quad (2.20)$$

and the remaining vertex $g_{\nu\nu_1\nu_2}(q^2)$ has a finite limit as $q^2 \rightarrow 0$:

$$g_{\mu\mu_1\mu_2}(0) = \frac{2\pi^2}{(2\pi)^6} \frac{\Gamma(1-\mu)}{\Gamma(\mu)} \frac{\Gamma(\mu_1)\Gamma(\mu_2)}{\Gamma(1-\mu_1)\Gamma(1-\mu_2)} \quad (2.21)$$

We mention that (2.18) can also be evaluated at $q^2 = 0$ directly. The result is

$$(2\pi)\delta(\mu_1 + \mu_2 - \mu)g_{\mu\mu_1\mu_2}(0) \quad (2.22)$$

Both the pole in (2.20) and the δ -function in (2.22) express the "conservation of conformal dimension μ "³: in (2.22) one sees it directly, whereas for (2.20) we will show further below that in the limit $q^2 \rightarrow 0$ the pole at $\mu = \mu_1 + \mu_2$ will dominate. This result will be shown to have interesting consequences for the energy dependence of the inclusive cross section in the triple Regge region at $t = 0$. Finally, we mention that (2.18) also contains terms without the singularity shown in (2.20): one can show that for small q^2 they vanish faster than the contribution coming from (2.20). Therefore, they will not be considered here.

We return to the partial wave in (2.17) and look at the implications of our result for (2.18). We still need to perform the integration over the variables μ, μ_1, μ_2 , using the saddle point approximation. The relevant terms are:

$$\int \int \int \frac{d\mu}{2\pi i} \frac{d\mu_1}{2\pi i} \frac{d\mu_2}{2\pi i} \frac{\left(\frac{q^2}{Q_0^2}\right)^{\mu_1+\mu_2-\mu}}{\mu - \mu_1 - \mu_2} \frac{e^{y(\chi(\mu_1)+\chi(\mu_2))}}{\mu + 1} \left(\frac{Q^2}{Q_0^2}\right)^\mu \quad (2.23)$$

where $y = \ln 1/x_B$ and $\chi(\mu_i) = \chi(0, \nu_i)$. The single pole at $\mu = -1$ arises from combining the double pole in (2.4) with the zero in (2.21). As q^2 is small we close the μ -contour to the left, obtaining the two contributions from the poles at $\mu = \mu_1 + \mu_2$ and $\mu = -1$:

$$\int \int \frac{d\mu_1 d\mu_2}{(2\pi i)^2} \left[\frac{\left(\frac{Q^2}{Q_0^2}\right)^{\mu_1+\mu_2}}{\mu_1 + \mu_2 + 1} - \frac{\left(\frac{q^2}{Q_0^2}\right)^{1+\mu_1+\mu_2} \left(\frac{Q^2}{Q_0^2}\right)^{-1}}{\mu_1 + \mu_2 + 1} \right] e^{y[\chi(\mu_1)+\chi(\mu_2)]}. \quad (2.24)$$

We restrict ourselves to the case $\ln(Q^2/Q_0^2) \ll y$. We begin with q^2 near Q_0^2 and perform the usual saddle point analysis. The main contribution comes from $\mu_1 = \mu_2 = -\frac{1}{2}$ (i.e. $\mu_1 + \mu_2 + 1$ is small), and the pre-exponent in (2.24) behaves as $\ln(Q^2/q^2)$:

$$(2.24) \sim \frac{Q_0^2}{Q^2} \ln\left(\frac{Q^2}{q^2}\right) \left(\frac{1}{x_B}\right)^{2\omega_{BFKL}} \frac{1}{2\pi \ln(1/x_B) \chi''(-1/2)} \quad (2.25)$$

with $\omega_{BFKL} = \chi(-1/2) = \frac{N_c \alpha_s}{\pi} 4 \ln 2$.

The q^2 -dependence in (2.25) seems to indicate that the expression diverges at $q^2 = 0$, but this is not the case. Namely, when $\ln Q_0^2/q^2$ becomes large (of the order of y or even larger), the saddle point analysis of (2.24) has to be modified. Starting with the first of the two terms, we introduce the variables $\mu_+ = \mu_1 + \mu_2$ and $\mu_- = \mu_1 - \mu_2$. For μ_- we again use the saddle point approximation,

³ The proof of conformal invariance is under consideration.

whereas for μ_+ we move the contour to the left (parallel to the imaginary axis with real part -1 , with a small semicircle to the right of the point $\mu_+ = -1$). The result of the μ_+ -integral comes only from the semicircle and equals half the residue (we note that the same result would have been obtained, if we would have used (2.22), i.e. putting directly $t = 0$ in (2.18)). As to the second term in (2.24), the saddle point analysis now has to take into account that there are two large parameters: writing the q^2 -factor as an exponential, we have y and $\ln Q_0^2/q^2$. With growing $\ln Q_0^2/q^2$, the saddle point conditions become

$$\chi'(\mu_1) = \chi'(\mu_2) = \frac{\ln Q_0^2/q^2}{y} \quad (2.26)$$

i.e. the saddle points of the μ_1, μ_2 integrals start to move away from $-1/2$ more and more towards $\mu_1 = \mu_2 = 0$. Consequently, in the limit $q^2 = 0$, the power of q^2 gets close to unity, and the term vanishes. Therefore, the small- t limit of (2.24) comes only from the first term and equals:

$$(2.24) = \frac{1}{4} \frac{Q_0^2}{Q^2} \left(\frac{1}{x_B}\right)^{2\omega_{BFKL}} \frac{1}{\sqrt{\pi \ln(1/x_B) \chi''(-1/2)}} [1 + O(\sqrt{\frac{\ln^2(Q^2/Q_0^2)}{\ln(1/x_B) \chi''}})] \quad (2.27)$$

This has to be compared with (2.25) which is valid only for nonzero momentum transfer ($\ln(Q_0^2/q^2) \ll y$). As a function of q^2 , we expect to see a strong variation: going from (2.25) to (2.27), the cross section grows but reaches a finite limit. A similar saddle point analysis of the q^2 -derivative of (2.23) shows that the derivative tends to infinity as $q^2 \rightarrow 0$: the cross section therefore develops a cusp at $t = 0$ (a more detailed discussion will be given further below).

To complete our analysis of (2.17) we have to couple the BFKL Pomerons to the proton. The \mathbf{l}' integral in the second line of (2.17) couples the second $E^{(\nu)}$ -factor of the BFKL Pomeron to the proton and, hence, belongs to nonperturbative physics. We assume that the limit $q^2 \rightarrow 0$ is finite and has no strong variation in the conformal dimensions μ_i . Furthermore, guided by the simple model (2.16) we expect that the coupling should scale as $(Q_0^2)^{-1/2-i\nu_i}$. As a result, the coupling of the BFKL Pomeron to the proton in the region of small t is taken as:

$$(Q_0^2)^{-1/2-i\nu_i} \frac{C}{2\sqrt{2}} \quad (2.28)$$

where C is the constant from (2.16), independent of μ_i and t .

Before we present our final formula for the cross section, we comment on the typical momentum scale at the upper end of the two BFKL ladders. Starting from the hadron vertex at the lower end where the average momentum lies in the vicinity of the hadronic scale Q_0^2 , we move upwards, and the distribution in transverse momentum evolves in accordance with the diffusion mechanism. At first sight one might expect that at the upper end the large scale of the photon mass $\sqrt{Q^2}$ forces the diffusion into the ultraviolet direction: this expectation, however, is not correct. Namely, if we consider the quark loop as the first cell of a GLAP evolution ladder which provides the biggest contribution to the cross section only if the difference between the momentum scales at the upper and lower end is as large as possible, then it becomes plausible that we have a competition between the GLAP dynamics from the quark loop and the BFKL diffusion mechanism from below. As a result, the scale at the upper end of the ladders is pushed into the infrared region. A computer analysis confirms this picture [11].

Collecting finally all our results, we arrive at the following expression for the cross section (2.1) at $t = 0$:

$$\left. \frac{d\sigma^{DD}}{dt} \right|_{t=0} = \sum_f \frac{2e_f^2 \alpha_{em} \alpha_s^2 C^2}{9Q^2 Q_0^2} \frac{1}{\sqrt{21\alpha_s \zeta(3)y}} \left(\frac{1}{x_B} \right)^{2\omega_{BFKL}}. \quad (2.29)$$

For comparison, we quote the result for the total cross section, calculated with the BFKL-ladders and the same coupling to the proton (Fig.3):

$$\sigma(\gamma^* + \text{proton}) = \sum_f \frac{e_f^2 \alpha_{em} \alpha_s C 9\sqrt{2}\pi^3}{64\sqrt{Q^2 Q_0^2}} \left(\frac{1}{x_B} \right)^{\omega_{BFKL}} \frac{\exp\left(\frac{-\pi(\ln Q_0^2/Q^2)^2}{4\alpha_s 42\zeta(3)y}\right)}{\sqrt{42\zeta(3)\alpha_s y}} \quad (2.30)$$

For a phenomenological analysis one might think of taking the ratio $\frac{d\sigma^{DD}}{dt}$ over σ and determining the unknown constant C from a fit to F_2 :

$$\left. \frac{1}{\sigma} \frac{d\sigma^{DD}}{dt} \right|_{t=0} = \frac{1}{\sum_f e_f^2} \frac{2^{15}}{3^6 \pi^4} \frac{\sqrt{21\zeta(3)\alpha_s y}}{Q^2} F_2 \quad (2.31)$$

In eq.(2.31) we have neglected corrections of the type $\ln(Q^2/Q_0^2)$. Taking $x_{Bj} = 10^{-3}$ and $Q^2 = 10\text{GeV}^2$ we find, as a quantitative prediction, that 10 % of the usual DIS-events are diffractively produced $q\bar{q}$ -pairs. This is clearly only a rough estimate, and its validity is restricted by the condition that the BFKL Pomeron has to be applicable. This excludes configurations where one of the quarks is soft, but, nevertheless, it turns out to be a reasonable value.

3 The Configuration Space Representation

In this section we present an alternative way of deriving the cross section for the diffractive $q\bar{q}$ -production. We consider the $q\bar{q}$ -final state as two opposite colour charges in the configuration or impact parameter space. The important parameter is their separation \mathbf{r} . This representation as Colour Dipole in the impact parameter space (see for example ref. [12, 13]) has the nice property that it diagonalizes the scattering matrix in the limit of high energy (small x) and small momentum transfer, i.e the impact parameter is a good quantum number. Multiple scattering turns out to be simply the product of single scattering due to which the calculation can be performed in a compact way and shows from the beginning the final factorized form as in eq. (2.18). We normalize the wave function $\Psi(\mathbf{r})$ using $D_{(2;0)}$ which was introduced in ref. [2]:

$$\begin{aligned} D_{(2;0)}(\mathbf{k}) &= \int d^2\mathbf{r} |\Psi(\mathbf{r})|^2 (1 - e^{i\mathbf{k}\cdot\mathbf{r}}) (1 - e^{-i\mathbf{k}\cdot\mathbf{r}}) \\ &= \int d^2\mathbf{r} |\Psi(\mathbf{r})|^2 (2 - e^{i\mathbf{k}\cdot\mathbf{r}} - e^{-i\mathbf{k}\cdot\mathbf{r}}) \end{aligned} \quad (3.1)$$

with

$$|\Psi(\mathbf{r})|^2 = \sum_f e_f^2 \alpha_s \frac{\sqrt{8}}{4\pi^2} \int_0^1 d\alpha [1 - 2\alpha(1 - \alpha)] \alpha(1 - \alpha) Q^2 K_1^2 \left(\sqrt{\alpha(1 - \alpha) Q^2 r^2} \right) . \quad (3.2)$$

K_1 is the modified Bessel function of first order. For comparison see ref. [12] and [13]. Next, we would like to generalize from two gluons to four gluons with each of the gluon pairs (1,2) and (3,4) in the colour singlet state. We can apply the same wave function as in eq.(3.1). One only needs to add two more factors of the type $(1 - e^{i\mathbf{k}\cdot\mathbf{r}})$, the corresponding colour factor and a g^2 for the coupling of two more gluons. Accordingly, we can rewrite $D_{(4;0)}$ as:

$$D_{(4;0)}(\mathbf{k}) = g^2 \frac{\sqrt{2}}{3} \int d^2\mathbf{r} |\Psi(\mathbf{r})|^2 (1 - e^{i\mathbf{k}_1\cdot\mathbf{r}}) (1 - e^{i\mathbf{k}_2\cdot\mathbf{r}}) (1 - e^{i\mathbf{k}_3\cdot\mathbf{r}}) (1 - e^{i\mathbf{k}_4\cdot\mathbf{r}}) \quad (3.3)$$

with $\mathbf{k}_1 + \mathbf{k}_2 + \mathbf{k}_3 + \mathbf{k}_4 = 0$. As before, we fix the momentum tranfer along the Pomeron $\mathbf{q} = \mathbf{k}_1 + \mathbf{k}_2 = -\mathbf{k}_3 - \mathbf{k}_4$. The notation for the internal transverse momenta of the left and right Pomeron were chosen to be $\mathbf{l} = \mathbf{k}_1$ and $\mathbf{m} = \mathbf{k}_3$. With this notation eq.(3.3) gives:

$$\begin{aligned} D_{(4;0)}(\mathbf{k}) &= g^2 \frac{\sqrt{2}}{3} \int d^2\mathbf{r} |\Psi(\mathbf{r})|^2 \left[1 - e^{i\mathbf{l}\cdot\mathbf{r}} + (1 - e^{-i\mathbf{l}\cdot\mathbf{r}}) e^{i\mathbf{q}\cdot\mathbf{r}} \right] \cdot \\ &\cdot \left[1 - e^{i\mathbf{m}\cdot\mathbf{r}} + (1 - e^{-i\mathbf{m}\cdot\mathbf{r}}) e^{-i\mathbf{q}\cdot\mathbf{r}} \right] . \end{aligned} \quad (3.4)$$

This expression is already factorized corresponding to each of the Pomerons.

It was shown in section 2 that with the help of the Pomeron-eigenfunction $E^{(\nu)}$ for a given momentum transfer \mathbf{q} the solution of the Lipatov equation can be factorized. The vertex g (see eq.(2.18)) is part of the projection of $D_{(4;0)}$ on these eigenfunctions. In the following we will use the mixed representation (2.15) of the Pomeron-eigenfunction $E^{(\nu)}$ and take the Fourier transformation of $D_{(4;0)}$. It is enough to look at one of the factors of (3.4) e.g. $[1 - e^{i\mathbf{l}\cdot\mathbf{r}} + (1 - e^{-i\mathbf{l}\cdot\mathbf{r}})e^{i\mathbf{q}\cdot\mathbf{r}}]$. Its Fourier transformed is $\delta(\rho) - \delta(\mathbf{r} + \rho) + [\delta(\rho) - \delta(\mathbf{r} - \rho)]e^{i\mathbf{q}\cdot\mathbf{r}}$ where the impact parameter ρ corresponds to \mathbf{l} . A crucial property of this expression is its vanishing after the integration over ρ . This reflects the colour cancellation and is an important requirement to restore the conformal invariance as was shown in [14]. Inserting the eigenfunction $E^{(\nu)}(\rho, \mathbf{q})$ and integrating over ρ we end up with

$$\begin{aligned} & g^2 \frac{\sqrt{2}}{3\pi^2} \int d^2\mathbf{r} |\Psi(\mathbf{r})|^2 E^{(\nu_1)}(\mathbf{r}, \mathbf{q}) E^{(\nu_2)}(\mathbf{r}, -\mathbf{q}) \\ &= g^2 \frac{\sqrt{2}}{3\pi^2} \int dr r |\Psi(r)|^2 \int_0^{2\pi} d\phi E^{(\nu_1)}(\mathbf{r}, \mathbf{q}) E^{(\nu_2)}(\mathbf{r}, -\mathbf{q}) . \end{aligned} \quad (3.5)$$

Note that $E^{(\nu)}$ vanishes when \mathbf{r} equals zero, and we have made use of the relation $E^{(\nu)}(\mathbf{r}, \mathbf{q}) e^{i\mathbf{q}\cdot\mathbf{r}} = E^{(\nu)}(-\mathbf{r}, \mathbf{q})$. In order to recover the vertex g in terms of the three conformal dimensions ν, ν_1 and ν_2 we have to take the Mellin transformation of the wave function:

$$\begin{aligned} & \int dr r |\Psi(r)|^2 r^{1+2i\nu} \\ &= \sum_f e_f^2 \alpha_s \frac{\sqrt{8} 4^{i\nu}}{16\pi} \frac{\Gamma(5/2 + i\nu)}{\Gamma(2 + i\nu)} \frac{\Gamma(1/2 + i\nu)}{1/2 + i\nu} \frac{\Gamma(1/2 - i\nu)}{1/2 - i\nu} \frac{\Gamma(5/2 - i\nu)}{\Gamma(2 - i\nu)} \frac{\Gamma(3/2 + i\nu)}{-\Gamma(-1/2 - i\nu)} \\ &= \frac{4^{i\nu}}{2\pi} \frac{\Gamma(3/2 + i\nu)}{-\Gamma(-1/2 - i\nu)} \tilde{D}_{(2;0)}(-1/2 - i\nu) \end{aligned} \quad (3.6)$$

$\tilde{D}_{(2;0)}$ is the Mellin transformed of $D_{(2;0)}$ in the momentum space (eq.(2.4)). The factor in front of $\tilde{D}_{(2;0)}$ is the inverse of a factor which follows from the Fourier transformation of $(k^2)^{-3/2-i\nu}$. This relation is illustrated by taking $E^{(\nu)}$ in the forward direction, i.e. at $\mathbf{q} = 0$ (see the discussion after (2.9)):

$$E^{(\nu)}(\rho, \mathbf{q} = 0) = \sqrt{2} 4^{-i\nu-1} \frac{-\Gamma(-1/2 - i\nu)}{\Gamma(3/2 + i\nu)} \rho^{1+2i\nu} \quad (3.7)$$

The vertex g which was defined in eq.(2.18) can now be rewritten in terms of the impact parameter

\mathbf{r} :

$$g_{\nu\nu_1\nu_2}(q^2) \frac{q^{-1+2i\nu-2i\nu_1-2i\nu_2}}{1/2-i\nu+i\nu_1+i\nu_2} = \frac{4^{i\nu}}{2\pi^3} \frac{\Gamma(3/2+i\nu)}{-\Gamma(-1/2-i\nu)} \int dr r^{-2i\nu-2} \int_0^{2\pi} d\phi E^{(\nu_1)}(\mathbf{r}, \mathbf{q}) E^{(\nu_2)}(\mathbf{r}, -\mathbf{q}) . \quad (3.8)$$

We are mainly interested in the limit $q^2 \rightarrow 0$ of expression (3.8). Following the discussion of section 2 we have to evaluate the residue at the point $1-2i\nu+2i\nu_1+2i\nu_2=0$, e.g.:

$$g_{\nu\nu_1\nu_2}(q^2) \frac{q^{-1+2i\nu-2i\nu_1-2i\nu_2}}{1/2-i\nu+i\nu_1+i\nu_2} \Big|_{q^2=0} = 2\pi \delta(1/2-i\nu+i\nu_1+i\nu_2) g_{\nu\nu_1\nu_2}(0) \quad (3.9)$$

Finally we can evaluate the vertex $g_{\nu\nu_1\nu_2}$ by partial integration:

$$\begin{aligned} g_{\nu\nu_1\nu_2}(0) &= \frac{4^{i\nu}}{2\pi^3} \frac{\Gamma(3/2+i\nu)}{-\Gamma(-1/2-i\nu)} \int dr (1-2i\nu+2i\nu_1+2i\nu_2) r^{-2i\nu+2i\nu_1+2i\nu_2} \\ &\cdot \int_0^{2\pi} d\phi r^{-1-2i\nu_1} E^{(\nu_1)}(\mathbf{r}, \mathbf{q}) r^{-1-2i\nu_2} E^{(\nu_2)}(\mathbf{r}, -\mathbf{q}) \\ &= \frac{1}{\pi^2} 4^{i\nu} \frac{\Gamma(3/2+i\nu)}{-\Gamma(-1/2-i\nu)} \left[r^{-1-2i\nu_1} E^{(\nu_1)}(\mathbf{r}, \mathbf{q}) \right]_{\mathbf{r}=0} \left[r^{-1-2i\nu_2} E^{(\nu_2)}(\mathbf{r}, -\mathbf{q}) \right]_{\mathbf{r}=0} \\ &= \frac{1}{8\pi^2} \frac{\Gamma(3/2+i\nu)}{-\Gamma(-1/2-i\nu)} \frac{\Gamma(-1/2-i\nu_1)}{\Gamma(3/2+i\nu_1)} \frac{\Gamma(-1/2-i\nu_2)}{\Gamma(3/2+i\nu_2)} \end{aligned} \quad (3.10)$$

The final result agrees with (2.21).

The main advantage of this derivation is its compact form and the absence of subtraction terms which make the calculation in the momentum space more involved. But, the calculation can only be performed at finite \mathbf{q} which serves as infrared cutoff whereas the momentum integrals in section 2 are finite at $\mathbf{q} = 0$.

4 The Triple Pomeron Vertex

We return to momentum space and consider the more general case of the inclusive cross section in the triple Regge region (Fig.4):

$$\frac{d^2\sigma}{dt dM^2} = \frac{1}{16\pi M^2} \int \frac{d\omega}{2\pi i} \int \frac{d\omega_1}{2\pi i} \int \frac{d\omega_2}{2\pi i} \left(\frac{s}{M^2} \right)^{\omega_1+\omega_2} \left(\frac{M^2}{Q^2} \right)^\omega F(\omega, \omega_1, \omega_2, 0, t, t) \quad (4.1)$$

where M denotes the invariant mass of the diffractively produced system. The analytical calculation of the partial wave F has been done in [2], and in this paper we study the change in the energy

dependence near $t = 0$. As the dependence upon s/M^2 and M^2/Q^2 is determined by the ω -singularities in the two lower legs and the upper t-channel, resp., we expect $\omega_1 = \omega_2 = \omega_{BFKL}$, and $\omega = \omega_4$ or $\omega = \omega_{BFKL}$ (ω_4 denotes the leading singularity of the four-gluon state). In [2] it was shown that the full inclusive cross section comes as a sum of two terms: in the first term (Fig.1b), the two lower BFKL ladders couple, via a disconnected vertex, to the upper BFKL ladder; consequently we expect $\omega = \omega_{BFKL}$. In the second term (Fig.1a), the two lower BFKL ladders first merge into a four-gluon state, where the four gluon lines interact in all possible ways; then there is a transition vertex from the four-gluon state to the two-gluon state, which has the familiar BFKL interaction kernels and connects to the fermion box at the top of the diagrams. As a result we have contributions from both $\omega = \omega_{BFKL}$ and $\omega = \omega_4$.

The following discussion we will show that these expectations for ω (and therefore the M^2 -dependence) are not correct when $t \rightarrow 0$: as a result of the conservation of conformal dimension found in (2.20) and (2.22), there is no coupling between the leading ω -singularities in all three channels, i.e. the coupling between the three BFKL-singularities generated by the three ladders in Fig.1b vanishes at $t = 0$. In Fig.1a our ignorance of the ω -singularity of the four-gluon state prevents us from carrying out a complete analysis: presently we can only conclude that the conservation of the conformal dimension holds and that the leading singularity (whatever it will be) decouples from the lower two BFKL-singularities. In any case, we predict a change in the M^2 -dependence near $t = 0$.

In analogy with the structure of the inclusive cross section, our following analysis goes in two steps. First we consider the first part, i.e. the direct coupling of three BFKL ladders. This part will be referred to as the “triple ladder vertex“, in order to distinguish this part from the full “triple Pomeron vertex“. In the second part we turn to the more complex case where the two BFKL-ladders couple to the four-gluon state; here our analysis will remain somewhat incomplete.

4.1 The Triple Ladder Vertex

The expression for Fig.1b can be obtained from (2.17) by simply replacing the fermion loop $D_{(4;0)}$ by the full sum of gluon ladders $D_{(4)}^R$ (in the notation on [2]). In analogy with (2.3) $D_{(4)}^R$ can also be written as a sum of seven terms: on the lhs of (2.3), we replace $D_{(4;0)}$ by $D_{(4)}^R$, and on the rhs all the $D_{(2;0)}$'s by the corresponding $D_{(2)}$'s. As reviewed in [18], the two-gluon function $D_{(2)}(\mathbf{k}, -\mathbf{k})$ has a representation analogous to (2.3). Singularities in the μ -plane are poles which lie at distances of order g^2 away from positive and negative integer μ -values. The integrations over \mathbf{l} and \mathbf{m} are done in the same way as described before ((2.20)), leading again to (2.20) and (2.22) for $t \neq 0$ and $t = 0$, resp. The evaluation of the remaining μ -integrals, however, is slightly different. Namely, instead of (2.23), we need to calculate

$$\int \int \int \frac{d\mu}{2\pi i} \frac{d\mu_1}{2\pi i} \frac{d\mu_2}{2\pi i} \frac{\left(\frac{q^2}{Q_0^2}\right)^{\mu_1+\mu_2-\mu}}{\mu - \mu_1 - \mu_2} \left(\frac{Q^2}{Q_0^2}\right)^\mu e^{y_M \chi(\mu) + y_s [\chi(\mu_1) + \chi(\mu_2)]} \quad (4.2)$$

where $y_M = \ln M^2/Q^2$ and $y_s = \ln s/M^2$. We consider the low mass region $y_M \ll y_s$ and take $\ln(Q^2/Q_0^2) \ll y_s$. The most interesting case is $y_M \leq \ln(Q^2/Q_0^2)$. We begin with q^2 being of the order Q^2 , where we simply repeat the standard saddle point analysis: one finds $\mu_{1S} = \mu_{2S} = -1/2$ and, as a condition on μ_S ,

$$0 = y_M \chi'(\mu_S) + \ln Q^2/q^2. \quad (4.3)$$

Since for q^2 near Q^2 $\ln Q^2/q^2$ will be small compared to y_M , we obtain

$$\mu_S = -\frac{1}{2} - \frac{\ln Q^2/q^2}{y_M \chi''(-\frac{1}{2})}. \quad (4.4)$$

The result for (4.2) is:

$$2 \frac{Q_0^2}{Q^2} \left(\frac{q^2}{Q^2}\right)^{-1/2} \left(\frac{s}{M^2}\right)^{2\omega_{BFKL}} \left(\frac{M^2}{Q^2}\right)^{\omega_{BFKL}} \frac{\exp(-\frac{\ln^2(Q^2/q^2)}{2y_M \chi''}) \exp(-\frac{\ln^2(q^2/Q_0^2)}{y_s \chi''})}{\sqrt{2\pi \chi''(-\frac{1}{2}) y_M} 2\pi \chi''(-\frac{1}{2}) y_s} \quad (4.5)$$

Here the q^2 -dependence agrees with what first has been found in [1]. Moving now to smaller q^2 -values, we come into the region near $q^2 = Q_0^2$ where $y_M \leq \ln Q^2/q^2 \ll y_s$, and the solution to (4.3) is no longer given by (4.4). Instead, μ_S moves close to -1 :

$$\mu_S = -1 - \sqrt{\frac{\alpha_s N_c y_M}{\pi \ln Q^2/q^2}} \quad (4.6)$$

which leads to the following result for (4.2):

$$\frac{Q_0^2}{Q^2} \exp \left(2y_s \omega_{BFKL} + 2\sqrt{\frac{N_c \alpha_s}{\pi}} y_M \ln \frac{Q^2}{q^2} \right) \left(16\pi N_c \alpha_s y_M \ln \left(\frac{Q^2}{q^2} \right) \right)^{-\frac{1}{4}} \frac{\exp(-\frac{\ln^2(q^2/Q_0^2)}{y_s \chi''})}{2\pi \chi''(-\frac{1}{2}) y_s} \quad (4.7)$$

We thus obtain, for the M^2 -dependence, the typical GLAP result for the upper ladder with q^2 as lower scale and starting point of the evolution.

Before we come to the third region $0 < q^2 < Q_0^2$ we mention, for completeness, also the other case, $\ln(Q^2/Q_0^2) \ll y_M$. For q^2 near Q^2 , the result of (4.2) is, again, given by (4.4); when q^2 moves close to Q_0^2 , the saddle point μ_S stays near $-1/2$ (eq.(4.4)), and (4.5) remains valid.

Finally the limit $q^2 \rightarrow 0$ ($q^2 < Q_0^2$). When in (4.5) the momentum transfer q^2 becomes smaller and smaller, we observe a similar phenomenon as described after (2.25): the effective power of q^2 increases from $-1/2$ to zero, and the limit $t = 0$ is finite. To see this in detail, we write $\left(\frac{q^2}{Q_0^2}\right)^{\mu_1 + \mu_2 - \mu} = \exp[(\mu - \mu_1 - \mu_2) \ln Q_0^2/q^2]$, and we search for the saddle point of the function:

$$\psi(\mu, \mu_1, \mu_2) = (\mu - \mu_1 - \mu_2) \ln Q_0^2/q^2 + y_M \chi(\mu) + y_s [\chi(\mu_1) + \chi(\mu_2)] + \mu \ln Q^2/Q_0^2 \quad (4.8)$$

The conditions are:

$$0 = \ln Q^2/q^2 + y_M \chi'(\mu_S) \quad (4.9)$$

$$0 = -\ln Q_0^2/q^2 + y_s \chi'(\mu_{iS}), \quad (4.10)$$

and one sees that for very small q^2 all saddle point values start to move: μ_S moves to the left (towards the point $\mu = -1$ where the function χ becomes infinite with a negative slope), whereas the μ_{iS} start to move in the right direction $\mu_{iS} > -1/2$ (at zero $\chi(\mu_i)$ tends to infinity with a positive slope). (4.9) and (4.10) also indicate at which q^2 -values the motion starts. For the μ_i , we need $\ln(Q^2/q^2)$ to become of the order y_M (which in case of $y_M \leq \ln(Q^2/Q_0^2)$ has already been reached for $Q_0^2 < q^2$, see above), whereas for μ the condition is $\ln(Q_0^2/q^2) \approx y_s$. In order to evaluate the integral (4.2), we shift the μ_i -contours to the right (such that it always passes through the saddle point), and we deform the μ -contour as shown in Fig.5. For $q^2 \rightarrow 0$ the saddle point approaches $\mu = -1$, $\mu_i = 0$ and the final result splits (4.2) into two contributions: the pole contribution which is independent of q^2 , and a q^2 -dependent part which can be computed from the saddle points in eqs.

(4.9) and (4.10). Since we look for saddle points close to $\mu_i = 0$ and $\mu = -1$, we can approximate the χ -function by its leading poles and find:

$$-\frac{q^2}{Q^2} \frac{\exp\left(2\sqrt{\frac{\alpha_s N_c}{\pi}} y_M \ln \frac{Q^2}{q^2}\right)}{2\left[\pi\alpha_s N_c y_M \ln \frac{Q^2}{q^2}\right]^{\frac{1}{4}}} \frac{\exp\left(4\sqrt{\frac{\alpha_s N_c}{\pi}} y_s \ln \frac{Q_0^2}{q^2}\right)}{4\sqrt{\pi\alpha_s N_c y_s \ln \frac{Q_0^2}{q^2}}} \quad (4.11)$$

(we remind that the starting point of our discussion, eq.(4.2), represents a somewhat simplified approximation to the partial wave in (4.1). In particular, the triple ladder vertex in (2.20) is valid only near the point $\mu = \mu_1 + \mu_2$. The full expression in (2.18) contains other poles at $\mu = \mu_1 + \mu_2 - 1, \dots$ which lead to contributions that are nonleading at small q^2 . Since (4.11) represents such a nonleading contribution, we should, in principle, have started from an approximation which is more accurate than (4.2) and contains also the pole at $\mu = \mu_1 + \mu_2 - 1$. However, the modification of (4.11) consists only of powers of y_s, y_M and $\ln(Q_0^2/q^2)$ in front of the exponential and is not essential for our discussion). Eq. (4.11) shows the familiar double leading log result: $\ln(M^2/Q^2) \ln(Q^2/q^2)$ for the upper ladder ($\mu \simeq -1$) with the usual ordering of the internal transverse momenta from the large scale Q^2 at the top down to the small scale q^2 , whereas the lower ladders dependent on the double logs $\ln(s/M^2) \ln(Q_0^2/q^2)$ with an inverse ordering ($\mu_i \simeq 0$) from the lower scale q^2 at the vertex up to the 'larger' scale Q_0^2 at the hadronic side of the diagram. It is easy to estimate the typical scale of transverse momenta at the triple ladder vertex: the contribution (4.11) will reach its maximum if the k_T^2 -evolution inside the ladders above and below are as long as possible: consequently, the momenta at the triple Pomeron vertex will try to be as small as possible, i.e. of the order of q^2 . This value should be rather independent of the energies. Although (4.11), by itself, vanishes as $q^2 \rightarrow 0$, it is nevertheless of physical interest since it determines the slope of the cross section near $t = 0$. The derivative of (4.11) becomes infinite at $t = 0$; for finite (but small) t it increases with both y_s and y_M . It should, however, be kept in mind that this large slope near $t = 0$, however, is due to very small momenta at the triple ladder vertex. In this region, predictions which are based upon a perturbative analysis are not reliable.

At $q^2 = 0$ expression (4.11) vanishes and only the second contribution, coming from the pole in the μ -plane at $\mu = \mu_1 + \mu_2$ gives a nonzero contribution (the exponent of q^2 in (4.2) equals zero).

The integrals over μ_1 and μ_2 are done using the saddle point approximation of the exponent:

$$\psi(\mu_1, \mu_2) = y_M \chi(\mu_1 + \mu_2) + y_s [\chi(\mu_1) + \chi(\mu_2)] + (\mu_1 + \mu_2) \ln Q^2 / Q_0^2 \quad (4.12)$$

We consider a few cases which we can treat analytically. The most interesting one is the low mass region $y_M \ll y_s$ which we have discussed also for $q^2 \neq 0$. The saddle point analysis distinguishes between the two regions:

$$(a) \quad y_s^2 y_M \gg \left(\ln \frac{Q^2}{Q_0^2} \right)^3 \quad (4.13)$$

$$(b) \quad y_s^2 y_M \ll \left(\ln \frac{Q^2}{Q_0^2} \right)^3 \quad (4.14)$$

The saddle points are :

$$(a) \quad \mu_{1S} = \mu_{2S} = -\frac{1}{2} + \left(\frac{N_c \alpha_s}{4\pi} \frac{1}{\chi''(-\frac{1}{2})} \frac{y_M}{y_s} \right)^{\frac{1}{3}} \quad (4.15)$$

$$(b) \quad \mu_{1S} = \mu_{2S} = -\frac{1}{2} + \sqrt{\frac{N_c \alpha_s}{4\pi} \frac{y_M}{\ln \frac{Q^2}{Q_0^2}}}, \quad (4.16)$$

and we obtain the following results for (4.2):

$$(a) \quad \frac{Q_0^2}{Q^2} \exp \left(2y_s \omega_{BFKL} + \frac{3}{2} \left(\frac{N_c \alpha_s y_M}{\pi} \right)^{\frac{2}{3}} \left[\frac{y_s \chi''(-\frac{1}{2})}{2} \right]^{\frac{1}{3}} \right) \frac{1}{\sqrt{12\pi} y_s \chi''(-\frac{1}{2})} \quad (4.17)$$

$$(b) \quad \frac{Q_0^2}{Q^2} \exp \left(2y_s \omega_{BFKL} + 2 \sqrt{\frac{N_c \alpha_s}{\pi} y_M \ln \frac{Q^2}{Q_0^2}} \right) \frac{1}{\sqrt{4\pi^2 y_s \chi''(-\frac{1}{2})}} \left(\frac{y_M}{\ln^3 \frac{Q^2}{Q_0^2}} \frac{N_c \alpha_s}{16\pi} \right)^{\frac{1}{4}} \quad (4.18)$$

Case (a) is the one which should be compared to our discussion for $q^2 \neq 0$ (4.5) and $y_M \leq \ln(Q^2/Q_0^2)$. We compare the results (4.5), (4.7), and (4.17), keeping the variables y_s , y_M , and Q^2/Q_0^2 fixed. Going from the point $q^2 = Q^2$ in (4.5) to $q^2 = Q_0^2$ in (4.7), we observe an increase (coming from the exponential) which depends upon the ratio $\ln(Q^2/Q_0^2)/y_M$. At $q^2 = 0$, (4.17) gives a finite value which, once more, is larger than (4.7). This last increase will depend upon y_s : the larger y_s , the stronger the enhancement. The change from the behavior (4.7) to (4.17) takes place when $\ln(Q_0^2/q^2)$ is of the order of y_s (see above).

Let us discuss some characteristic features of this pole contribution to (4.2). A typical property of the small mass region ($y_M \ll y_s$) is the location of the saddle point of $\mu = \mu_1 + \mu_2$ close to

-1. In this region the pole term of the first χ -function in eq. (4.12) dominates, i.e the transverse momenta of the upper ladder are strongly ordered. So the physics inside the upper ladder is the same as discussed after (4.11): the internal transverse momentum decreases (strongly ordered) as we move down from the photon to the triple ladder vertex. The two lower ladders, on the other hand, remain in the BFKL-region (μ_1 and μ_2 are close to $-1/2$), and we have the usual diffusion in $\ln(k_T^2/Q_0^2)$ inside the ladders. If we ask for the typical momentum scale at the triple ladder vertex, we recognize two competing effects: the upper ladder with its strong ordering tries to have as much evolution as possible, i.e. tends to lower the momentum at the triple ladder vertex. From below, on the other hand, we have two (approximately) gaussian distributions in $\ln(Q_0^2/k_T^2)$ which are centered at the hadronic scale Q_0^2 , have a width of the order y_s and, in particular, suppress the region of very small momenta. Convoluting these gaussians with the distribution from above, we find a maximum at $\ln(Q_0^2/k_T^2) = (y_M y_s^2)^{\frac{1}{3}} + \frac{2}{3} \ln(Q^2/Q_0^2)$. Consequently, for large energies the average momentum value at the triple ladder vertex is small and decreases with the energy:

$$\langle k_T^2/Q_0^2 \rangle \sim \exp(-const \cdot (y_M y_s^2)^{\frac{1}{3}}). \quad (4.19)$$

One therefore expects that with increasing energy the diffusion enters more and more into the infrared region where perturbation theory becomes unreliable. The two lower “hard“ Pomerons, therefore, from which our analysis had started, should more and more transform themselves into “soft“ (nonperturbative) ones.

Summarizing our discussion of case (a), our analysis of (4.2) (which is proportional to the inclusive cross section) consists of two pieces: the leading one (4.17) determines the size of the cross section at $t = 0$. The first nonleading term (4.11) vanishes at $t = 0$, but it determines the slope which becomes infinite at $t = 0$. So our cross section, as a function of t , has a cusp at $t = 0$. Since the slope increases with y_s , the width of the cusp shrinks with increasing energy. This situation is reminiscent of the two gluon exchange discussed in [20]: the result for the cross section is finite, but the slope at $t = 0$ is infinite, too. But our result differs from the simpler case of [20] in that our cusp has an energy dependent width. The physical origin for this kind of “shrinkage“ lies in the exponential factors in (4.11), i.e. the GLAP evolution above and below the triple ladder

vertex. The analysis of the typical momentum scale at the triple ladder vertex indicates that, within our purely perturbative analysis, more credibility should be given to the value of the cross section at $t = 0$ rather than to its slope near $t = 0$ which has been found to be a large distance effect.

The case (b) does not require much new discussion: at the triple ladder vertex we again have the competition between the GLAP ordering from above and the diffusion from below. The very large photon mass now tries to pull the momenta towards large values; but it turns out that the momentum scale at the central vertex never exceeds the hadronic scale Q_0^2 :

$$\langle \ln(k_T^2) \rangle \sim \ln(Q_0^2). \quad (4.20)$$

So the lower Pomerons again like to become nonperturbative, although somewhat less than in the case (a).

Finally we also mention a few results on the large mass region near $t = 0$. We consider the two cases:

$$(c) \quad y_M = y_s \gg \ln \frac{Q^2}{Q_0^2} \quad (4.21)$$

$$(d) \quad y_M \gg y_s \gg \ln \frac{Q^2}{Q_0^2} \quad (4.22)$$

In the first case, we find the stationary point near $\mu_1 = \mu_2 = -1/3$ and $\mu = -2/3$, in the second case near $\mu_1 = \mu_2 = -1/4$ and $\mu = -1/2$. The conditions are:

$$(c) \quad \mu_{1S} = \mu_{2S} = -\frac{1}{3} \quad (4.23)$$

$$(d) \quad \mu_{1S} = \mu_{2S} = -\frac{1}{4} - \frac{y_s \chi'(-\frac{1}{4})}{2y_M \chi''(-\frac{1}{2})} \quad (4.24)$$

They lead to the results:

$$(c) \quad \left(\frac{Q_0^2}{Q^2}\right)^{\frac{2}{3}} \exp\left(y_M \chi(-\frac{2}{3}) + 2y_s \chi(-\frac{1}{3})\right) \frac{1}{\sqrt{4\pi^2 y_s \chi''(-\frac{1}{3})}} \frac{1}{\sqrt{y_s \chi''(-\frac{1}{3}) + 2y_M \chi''(-\frac{2}{3})}} \quad (4.25)$$

$$(d) \quad \sqrt{\frac{Q_0^2}{Q^2}} \exp\left(y_M \omega_{BFKL} + 2y_s \chi(-\frac{1}{4})\right) \frac{1}{\sqrt{8\pi^2 y_M y_s \chi''(-\frac{1}{2}) \chi''(-\frac{1}{4})}}. \quad (4.26)$$

The values of the χ -functions are:

$$(c) \quad \chi(-\frac{1}{3}) = \chi(-\frac{2}{3}) = \frac{N_c \alpha_s}{\pi} 3 \ln 3 \approx 0.59 \quad (4.27)$$

$$(d) \quad \chi(-\tfrac{1}{4}) = \frac{N_c \alpha_s}{\pi} 6 \ln 2 \approx 0.75 \quad (4.28)$$

We briefly discuss some properties of these results. Most striking is the change in the power behavior in both s and M^2 . Compared with both (4.17) or (4.18), the coefficients of y_M and y_s have increased (cf.(4.27) and (4.28)): both values of the χ -function are larger than $\omega_{BFKL} = \chi(-\tfrac{1}{2}) = \frac{4N_c \alpha_s}{\pi} 4 \ln 2 \approx 0.5$). Translating this into powers of s and M^2 , we obtain:

$$(c) \quad \frac{d^2 \sigma}{dt dM^2} \sim s^{2\chi(-\frac{1}{3})} (M^2)^{-1-\chi(-\frac{1}{3})} \quad (4.29)$$

$$(d) \quad \frac{d^2 \sigma}{dt dM^2} \sim s^{2\chi(-\frac{1}{4})} (M^2)^{-1+\chi(-\frac{1}{4})-2\chi(-\frac{1}{2})}. \quad (4.30)$$

In contrast to the low-mass region (cases (a) and (b)), the momentum distribution at the triple ladder vertex is now a result of diffusion in $\ln(k_T^2)$ from both the upper and the two lower ladders. Combining this with the conservation law $\mu = \mu_1 + \mu_2$, we find that the scale at the triple ladder vertex behaves as:

$$(c) \quad \left\langle \frac{k_T^2}{Q_0^2} \right\rangle \sim \left(\frac{Q^2}{Q_0^2} \right)^{1/3} \cdot \exp(-y_s \chi'(-\tfrac{1}{3})) \quad (4.31)$$

$$(d) \quad \left\langle \frac{k_T^2}{Q_0^2} \right\rangle \sim \exp(-y_s \chi'(-\tfrac{1}{4})). \quad (4.32)$$

Again we find that the typical momentum scale at the triple ladder tends to be smaller than Q_0^2 . We finally mention that for large $\ln(Q_0^2/Q^2)$ the momentum scale reaches, as the limiting value, Q_0^2 , i.e. it will never get large.

4.2 The Four Gluon State

So far our discussion had been restricted to the first part of the triple Regge cross section (Fig.1b), the triple ladder vertex. We now turn to the contributions of Fig.1a. With our present understanding of the four gluon state we are not yet able to calculate the cross section analytically: the main obstacle is our ignorance of the leading ω -plane singularity of the four gluon state. Therefore we shall limit ourselves to a qualitative discussion of the small- t behavior. We first rearrange the interactions of the four gluon state as shown in Fig.6a: first sum over all rungs in the channels (12) and (34), then switch to the channels (13) and (24) etc. For the transition vertex 2 gluons

$\rightarrow 4$ gluons which has been derived and discussed in [2] we only need to know the following two features: (i) it vanishes as any of the four lower gluon momenta goes to zero; (ii) it possesses a scaling property: when coupled to the BFKL ladders above and the two Pomerons below (to be more precise: the upper $E^{(\nu)}$ -functions of the two BFKL-Pomerons), its dependence upon q_1 is simply a factor $(q_1^2)^{\mu_1+\mu'_1-\mu}$. The internal integrations converge as long as $\mu > \mu_1 + \mu_2$, and for $\mu = \mu_1 + \mu_2$ we get the familiar pole

$$\frac{1}{\mu - \mu_1 - \mu'_1} \quad (4.33)$$

We have not yet attempted to calculate the coefficient, since our discussion of this part will have to remain qualitative anyhow. For each “switch“ from the channels (ij), (kl) to (ik), (jl) or (il), (jk) (Fig.6b) we have an effective (momentum dependent) vertex which scales as

$$(q_i^2)^{-1-\mu_i-\mu'_i+\mu_{i+1}+\mu'_{i+1}} W(q_{i+1}^2/q_i^2). \quad (4.34)$$

Let us say a few words about the function $W(q_{i+1}^2/q_i^2)$. In the ultraviolet region the internal momentum integral converges as $dk^2/(k^2)^2$. In the infrared region a potential divergence could come from the region where one of the internal lines (for example, line a in Fig.6b) becomes soft. As long as the lower momenta (q_{i+1} in Fig.6b) is nonzero, we have the delta function pieces from both the Pomeron above and below which, at first sight, seem to be ill-defined. However, including the amputating factor k^2 and using the regularization given in (2.12), we obtain the behavior

$$dk^2 \frac{\lambda^2}{(k^2)^{1-2\lambda}} \quad (4.35)$$

In the limit $\lambda \rightarrow 0$ we have two zeros in the numerator, the singularity at $k^2 = 0$ is integrable, and the whole integral remains finite. When the lower momentum q_{i+1} is taken to zero (i.e. in Fig.6b the lower Pomerons are in the forward direction and behave as $(k^2)^{-3/2-i\nu/2}$ (eq.(2.9)), both lines a and b become soft simultaneously. Including the δ -function pieces from the upper two BFKL Pomerons, the k -integral diverges as $(q_{i+1}^2)^{-1/2-i\nu}$, but is multiplied by two λ -factors. As a result, this divergent contribution drops out, and the nonvanishing result comes from the nonsingular pieces of the BFKL vertices. Hence W is a well-defined function, and, in particular, $W(0)$ is finite.

From these simple arguments alone it already follows that the four gluon state in Fig.6a has the following pattern of momentum integrals (Fig6.c) :

$$\int_0^\infty dq_1^2 \dots dq_n^2 \frac{1}{\mu - \mu_1 - \mu'_1} (q_1^2)^{-1-\mu+\mu_2+\mu'_2} W\left(\frac{q_2^2}{q_1^2}\right) \dots (q_n^2)^{-1-\mu_n-\mu'_n+\mu_l+\mu_r} W\left(\frac{q^2}{q_n^2}\right) \quad (4.36)$$

Introducing the new variables $\xi_1 = q_1^2/q_2^2$, ..., $\xi_n = q_n^2/q^2$ we obtain:

$$\int_0^\infty \frac{d\xi_1}{\xi_1} \dots \frac{d\xi_n}{\xi_n} \frac{1}{\mu - \mu_1 - \mu'_1} \xi_1^{\mu_1+\mu'_1-\mu} \dots \xi_n^{\mu_l+\mu_r-\mu} W\left(\frac{1}{\xi_1}\right) \dots W\left(\frac{1}{\xi_n}\right) (q^2)^{\mu_l+\mu_r-\mu}. \quad (4.37)$$

As long as $\mu > \mu_i + \mu'_i$ the ξ -integrals are finite, both in the ultraviolet and infrared region. At $q^2 = 0$, the we put $\xi_n = q_n^2/Q_0^2$, and the integral over ξ_n leads to the conservation law $\delta(\mu - \mu_l - \mu_r)$.

In order to illustrate how the the saddle point argument works in the limit $q^2 = 0$ we restrict ourselves to the case with only one two-Pomeron state above (Fig.7). To see the interplay between the single BFKL and the two-BFKL state, it will be useful to keep the rapidity variable at the $2 \rightarrow 4$ gluon transition vertex. Instead of (4.2) we now have:

$$\int_0^{y_M} dy'_M \int \int \int \int \int \frac{d\mu}{2\pi i} \frac{d\mu_1}{2\pi i} \frac{d\mu'_1}{2\pi i} \frac{d\mu_l}{2\pi i} \frac{d\mu_r}{2\pi i} \frac{\left(\frac{q^2}{Q_0^2}\right)^{\mu_l+\mu_r-\mu} \left(\frac{Q^2}{Q_0^2}\right)^\mu}{(\mu - \mu_1 - \mu'_1)(\mu - \mu_l - \mu_r)} \cdot e^{(y_M - y'_M)\chi(\mu) + y'_M[\chi(\mu_1) + \chi(\mu'_1)] + y_s[\chi(\mu_l) + \chi(\mu_r)]} \quad (4.38)$$

First, we consider q^2 to be of the order of Q^2 . In this region eq.(4.38) receives, from the nonforward coupling of the lower Pomerons to the proton, an extra factor $\left(\frac{Q^2}{Q_0^2}\right)^{-\mu_l-\mu_r}$, and the Q^2 dependence drops out. As a result, the saddle point is solely determined by the exponent $\exp((y_M - y'_M)\chi(\mu) + y'_M[\chi(\mu_1) + \chi(\mu'_1)] + y_s[\chi(\mu_l) + \chi(\mu_r)])$. The saddle point analysis is simple and yields the value $\mu_S = \mu_{1S} = \mu'_{1S} = \mu_{lS} = \mu_{rS} = -1/2$. Inserting this value we find $\exp([y_M + y'_M + 2y_s]\omega_{BFKL})$ which reaches its maximum at $y'_M = y_M$, i.e. the two-BFKL state gets all the available rapidity. In the same way the four gluon bound state will dominate over the single BFKL-singularity which leads to a new power-behaviour in M^2/s .

If we take, now, q^2 to be of the order of Q_0^2 , we have to perform a more accurate saddle point analysis. Introducing $\mu_{lS} = \mu_{rS} = \mu_{lrS}$ and $\mu_{1S} = \mu'_{1S} = \mu'_S$ we find the following equations:

$$0 = -\chi(\mu_S) + 2\chi(\mu'_S) \quad (4.39)$$

$$0 = y'_M \chi(\mu'_S) \quad (4.40)$$

$$0 = y_s \chi(\mu_{lrS}) \quad (4.41)$$

$$0 = (y_M - y'_M) \chi'(\mu_S) + \ln(Q^2/q^2) \quad (4.42)$$

The second and third equations yield $\mu'_S = \mu_{lrS} = -1/2$. The first equation then is solved by μ_S which lies between $-1/2$ and -1 . This saddle point gives the dominant behaviour as long as y_M exceeds the “critical” value

$$y_{Mc} = \frac{\ln(Q^2/Q_0^2)}{|\chi'(\mu_S)|}. \quad (4.43)$$

For y'_M we then find:

$$y'_M = y_M - y_{Mc}. \quad (4.44)$$

If y_M is smaller than y_{Mc} , y'_M stays at zero, i.e the two-BFKL state has zero rapidity and becomes a subleading correction to the single BFKL ladder above the two-BFKL state. Hence we are back to the three-ladder case discussed before. In particular, if y_M gets small in comparison with $\ln Q^2/Q_0^2$, the saddle point value μ_S slides down towards -1 , and the usual GLAP-dynamics takes over.

In the limit $t \rightarrow 0$ we return to (4.38) and perform the μ -integral. Closing the contour to the left, we have the two poles:

$$\int_0^{y_M} dy'_M \int \int \int \int \frac{d\mu_1}{2\pi i} \frac{d\mu'_1}{2\pi i} \frac{d\mu_l}{2\pi i} \frac{d\mu_r}{2\pi i} \frac{e^{y'_M[\chi(\mu_1)+\chi(\mu'_1)]+y_s[\chi(\mu_l)+\chi(\mu_r)]}}{\mu_l + \mu_r - \mu_1 - \mu'_1} \left(\left(\frac{Q^2}{Q_0^2} \right)^{\mu_l + \mu_r} e^{(y_M - y'_M)\chi(\mu_l + \mu_r)} - \left(\frac{Q^2}{Q_0^2} \right)^{\mu_1 + \mu'_1} \left(\frac{q^2}{Q_0^2} \right)^{\mu_l + \mu_r - \mu_1 - \mu'_1} e^{(y_M - y'_M)\chi(\mu_1 + \mu'_1)} \right) \quad (4.45)$$

We will now show that, at $t = 0$, only the first term survives; to this end we study the saddle points of each term separately. We begin with the first one. Putting again $\mu_l S = \mu_r S = \mu_{lrS}$, $\mu_1 S = \mu'_1 S = \mu'_S$, the saddle point conditions are:

$$0 = -\chi(2\mu_{lrS}) + 2\chi(\mu'_S) \quad (4.46)$$

$$0 = y'_M \chi(\mu'_S) \quad (4.47)$$

$$0 = (y_M - y'_M) \chi'(2\mu_{lrS}) + y_s \chi'(\mu_{lrS}) + \ln(Q^2/Q_0^2) \quad (4.48)$$

The second equation is solved if $\mu'_S = -1/2$ (the other possibility $y'_M = 0$ will be discussed in a moment). The first equation then is solved by a value μ_{lrS} which lies between $-1/2$ and $-1/3$. As long as y_M exceeds (“large-M region”) the value

$$y_{Mc} = \frac{y_s \chi'(\mu_{lrS}) + \ln(Q^2/Q_0^2)}{|\chi'(2\mu_{lrS})|}, \quad (4.49)$$

eq.(4.48) has the solution

$$y'_M = \frac{y_M |\chi'(2\mu_{lrS})| - y_s \chi'(\mu_{lrS}) - \ln(Q^2/Q_0^2)}{|\chi'(2\mu_{lrS})|} \quad (4.50)$$

In other words, the rapidity y_M is distributed between the single BFKL Pomeron and the two-Pomeron state in a very characteristic way. To obtain a result for the first part of (4.45) we put y'_M equal to the value given in (4.50) and use the saddle point approximation for the μ -integrals. The result is proportional to:

$$\exp \left[2y_s \chi(\mu_{lrS}) + 2y_M \omega_{BFKL} + 2\mu_{lrS} \ln(Q^2/Q_0^2) \right] \quad (4.51)$$

Note that the coefficient y_s is bigger than the “naive” expectation $2\omega_{BFKL}$. When y_M is lowered and reaches y_{Mc} , the saddle point value y_{MS} moves down to zero, i.e. the single BFKL Pomeron state gets the full available rapidity y_M . Now we are in a situation analogous to the triple ladder approximation of the previous subsection: the two-BFKL state becomes a subleading correction to the triple ladder vertex. When y_M further decreases (or, alternatively, either Q^2 or y_s become large), eqs.(4.46) and (4.48) can no longer be satisfied: the maximum of the exponent in (4.45) stays at $y'_M = 0$, and μ_{lrS} slides down towards $-1/2$:

$$\begin{aligned} \mu_{lrS} &= -\frac{1}{2} + \frac{1}{2} \left(\frac{2y_M \alpha_s N_c}{y_s \pi \chi''(-1/2)} \right)^{\frac{1}{3}} \quad \text{if} \quad \ln(Q^2/Q_0^2) \ll \left(y_M y_s^2 \chi'(-\frac{1}{2})^2 \frac{\alpha_s N_c}{4\pi} \right)^{\frac{1}{3}} \\ \mu_{lrS} &= -\frac{1}{2} + \frac{1}{2} \sqrt{\frac{y_M \alpha_s N_c}{\pi \ln(Q^2/Q_0^2)}} \quad \text{if} \quad \left(y_M y_s^2 \chi'(-\frac{1}{2})^2 \frac{\alpha_s N_c}{4\pi} \right)^{\frac{1}{3}} \ll \ln(Q^2/Q_0^2) \end{aligned} \quad (4.52)$$

which is identical to the triple ladder case (4.15) and (4.16).

As to the second term in (4.45), the analysis is very similar to the previous ones, and we can be brief in describing the main results. The saddle point value μ_{lrS} follows from the condition

$$0 = y_s \chi'(\mu_{lrS}) - \ln(Q_0^2/q^2), \quad (4.53)$$

i.e. it starts at $-1/2$ and tends towards zero, as q^2 becomes smaller and smaller. Again, there is a “critical” value of y_M :

$$y_{M\,c} = \frac{\ln(Q^2/q^2)}{|\chi'(2\mu'_S)|} \quad (4.54)$$

where μ'_S satisfies

$$\chi(2\mu'_S) = 2\chi(\mu'_S). \quad (4.55)$$

For $y_M > y_{M\,c}$ (or, alternatively, moderate Q^2 and finite q^2), the maximal contribution belongs to some $0 < y'_M < y_M$, i.e. the rapidity spreads over both the single and double BFKL state. The power of q^2 is negative:

$$\mu_l + \mu_r - \mu_1 - \mu'_1 \approx 2\mu_{lr\,S} - 2\mu'_S < 0 \quad (4.56)$$

and the overall sign of the second term in (4.45) is positive. For $y_M < y_{M\,c}$ (or, alternatively, smaller and smaller q^2), the maximum comes from $y'_M = 0$; the saddle point μ_S is now close to zero, and μ'_S moves towards $-1/2$. As a result the exponent of q^2 approaches $+1$, and the term vanishes $\sim q^2$.

Finally we wish to say a few words about the general case where the iteration of the two-Pomeron states above the vertex generates a new singularity in the ω -plane. The structure of (4.36) shows that the conservation of conformal spin at $t = 0$ works for any iteration of the two-BFKL cut. Guided by the calculation of the anomalous dimension of the four-gluon operator [18, 19] one may speculate that the new singularity lies to the right of the two-BFKL cut, i.e. $\omega_4 > 2\omega_{BFKL}$. As long as the corresponding saddle point value of μ is different from -1 (we expect it again to be at $\mu = -1/2$), the coupling of this new singularity to the lower BFKL-singularities will have the same features as in the triple ladder case, and we expect (qualitatively) the same physical picture. To be concrete we expect an expression similar to eq.(4.2), with $\chi(\mu)$ being replaced by another, so far unknown function of μ . For the low mass region, the dominant behavior near $t = 0$ is given by the point $\mu = -1$, where GLAP-like evolution holds. Consequently, the four gluon state will provide only some (not so interesting) corrections to the triple ladder picture (the higher-twist part of the four gluon state belongs to $\mu = -2$ and is not important for our discussion here). In the

large- M^2 region the saddle point in μ will move away from -1 to some finite value between -1 and 0, in analogy with (4.23), (4.24). Because of the higher intercept, the four gluon state will obtain the full rapidity y_M , whereas the single-BFKL state acts like a direct coupling of the four gluon system to the fermion loop. Furthermore, in this region of y_M the contribution of the four gluon state will dominate over the triple ladder part.

4.3 Summary

Let us try to summarize the results obtained in this section. Starting at some value away from $t = 0$, say $q^2 = -t$ of the order of the hadronic scale Q^2 , our cross section formula will be dominated by the leading ω -plane singularities above and below the triple vertex. In the upper t-channel the leading singularity is given by the four gluon state - either the two-BFKL state or a new four gluon bound state with intercept $\omega_4 > 2\omega_{BFKL}$ -, whereas in the lower Pomeron we have the usual BFKL singularity at $\omega = \omega_{BFKL}$. In this region of momentum transfer t one observes a negative power of t , i.e. the cross section grows with decreasing $-t$ as $1/\sqrt{-t}$. As to the momentum scale at the triple vertex, we have the usual diffusion picture in all three t-channels. In all three Pomerons, the diffusion into the infrared region is stopped by the momentum transfer $t \sim Q^2$, only a small contribution might come from the region at or below the hadronic scale Q_0^2 unless the photon mass Q^2 is too small (of the order of Q_0^2).

As t approaches zero, several changes occur. First of all, the negative power of t starts to move towards positive values: the initial rise with t comes to stop, and the cross section reaches a finite limit. At $t = 0$, the dependence upon s and M^2 becomes rather involved. Most striking, there is no simple uncorrelated energy dependence, but, the powers of s and M^2 change with the kinematic region. To begin with the small- M region (the precise condition is given in (4.44)), the upper gluon system is determined by GLAP dynamics, i.e. we have a clean twist-two state with strong ordering in the transverse momentum. The lower Pomerons are to be evaluated in the BFKL limit and the singularity at ω_{BFKL} describes the s dependence. In particular, the four-gluon state above the triple vertex is nonleading: it serves merely as a renormalization of the triple ladder vertex discussed in the first part. The typical momentum scale at the triple ladder vertex arises from the competition

between the strong ordering dynamics above and the diffusion mechanism from below: the former one tends to push the average scale into the infrared region, even below the hadronic scale Q_0^2 .

The large- M region, on the other hand, has quite different characteristics. Generally speaking, now the four gluon state above the triple vertex is equally or even more important than the simple triple ladder vertex. We therefore have to consider the contribution of the two-BFKL singularity and, in case it exists, also the formation of a new bound state to the right of $2\omega_{BFKL}$. In more detail, due to the conservation in μ (conformal dimension), the leading ω singularities in the upper and the lower Pomerons are linked together which implies, for the lower Pomerons, that the leading ω is larger than ω_{BFKL} . The amount by which the singularities are shifted towards larger values, depends upon the way in which the total available rapidity is distributed between the missing mass ($y_M = \ln(M^2/Q^2)$) and the rapidity gap ($y_s = \ln(s/M^2)$). One of the main conclusions of this analysis of the energy dependence therefore is that *the way in which the BFKL Pomeron contributes depends upon its environment*.

5 Discussion and Conclusions

In this paper we have obtained first analytic results on the rather complicated cross section formula for the diffractive dissociation of the photon in deep inelastic scattering of [2]. Our main interest was the behaviour near $t = 0$: for several reasons we expect this point to be particularly “dangerous” for the validity of perturbation theory. As one of the main results of our investigation we have found that, within the BFKL approximation, the cross section is finite at zero momentum transfer $t = -q^2 = 0$. At the same time, however, the $\ln k_t^2$ diffusion has penetrated deeply into the infrared region, and the typical transverse momentum at the triple Pomeron vertex is fairly small. Consequently, the BFKL approximation used in [2] provides a well-defined starting point for a systematic unitarization procedure, but it also emphasises the need for including higher order unitarizing corrections. Performing a careful saddle point analysis of our cross section formula we have also found very special features of the dependence upon s and M^2 near $t = 0$. As a function

of t , the cross section has a cusp-structure, and the cusp shrinks with increasing energy. The origin of these phenomena can be traced back to the conservation of conformal dimensions which relates to one of the profound properties of the BFKL approximation.

Although our main interest concerns the limit $t = 0$, it is instructive to extend our discussion to the region of nonzero t . We consider the triple Regge limit with $\ln(Q^2/Q_0^2)$ being of the order of $\ln(M^2/Q^2)$. Starting with t of the order of Q^2 , we find that the upper part of the diagram 1a,1b is governed by the usual diffusion of the internal transverse momenta around Q^2 . This kinematic region leads to the $1/\sqrt{-t}$ -behaviour of the cross section [1], and in the simplest case of only three ladders to the coupling of the three BFKL-singularities. New in our analysis is the four gluon state above the junction of the two lower Pomerons: it contains the two-BFKL state, but we expect that also a new bound state to the right of the two-BFKL singularity will be formed. Both the two-BFKL state and the new bound state will dominate the single-BFKL state, and we expect a different, new dependence on M^2 which may be measured in future.

Decreasing $-t$ down to Q_0^2 we have to distinguish between two different cases: the “high mass region“ ($\ln M^2/Q^2$ larger than $\ln Q^2/Q_0^2$) and the “low mass region“ ($\ln M^2/Q^2$ smaller than $\ln Q^2/Q_0^2$); the more precise definition is given in section 4 (eq.(4.43)). In the former case we are still in diffusion region, and the four gluon state plays an important role. In the second case, however, the case of not so large M^2 , we enter the GLAP region where the single BFKL ladder gives a larger contribution than the two-BFKL state or the new bound state since both contributions are subleading in $\ln(Q^2/Q_0^2)$. Now the dynamic of the evolution has changed crucially from diffusion (which includes all higher twist contributions) to the usual GLAP-evolution and the dominance of the leading twist piece. Furthermore, the M^2 -dependence experiences a change which should be measurable.

The advantage of considering first the region $t \neq 0$ (before moving towards $t = 0$) is that the BFKL diffusion stays away from the infrared region, and the use of perturbation theory is better justified. From this point of view it would be even more advantageous to move into the large t -region, $-t \gg Q^2$. A kinematic configuration of this type is realized in the diffractive vector meson

production as discussed in ref. [21] (see also ref.[22]). The approach in ref. [2] is general enough to be also applicable for this process. One only needs to substitute the corresponding wave functions of the initial particles and has to carry out an analysis quite analogous to the one outlined in this paper. The major difference becomes visible when trying to perform the saddle point analysis: for $q^2 = -t \rightarrow \infty$ (as opposed to: $q^2 \rightarrow 0$) the μ contours have to be closed in the opposite direction, and other singularities become relevant. The large- t limit, therefore, requires a separate investigation.

Returning to $t = 0$ we again have the two regions of low and high mass M (the precise definition is in (4.49) and now also depends upon $\ln(s/M^2)$). As before, the high mass region is characterized by the diffusion dynamics, and the four gluon state plays an important role, whereas the low mass region is governed by the single BFKL ladder in the GLAP region. At the same time, however, we face the problem that the typical momentum scale at the Triple Pomeon vertex lies far in the infrared region where leading order perturbation theory becomes unreliable and we should compute higher order correction. At the moment, therefore, we can only guess what the “true“ QCD behavior will be. Here a comparison of the small- x behavior of F_2 at large Q^2 with the high energy behavior of the photoproduction total cross section may be helpful. For sufficiently large Q^2 , it seems quite adequate to use the BFKL-approximation for the x -dependence of F_2 , since the main contribution of the momentum integrals comes from the ultraviolet region; the result of this is the well-known power behavior $F_2 \sim (1/x)^{\omega_{BFKL}}$. When we lower Q^2 , the contribution of small internal momenta becomes larger and we should include more and more corrections to the BFKL-approximation; eventually, nonperturbative effects will take over. On the other hand we know that at $Q^2 = 0$ (the photoproduction limit) the energy dependence is much weaker ($\sigma_{tot}(\gamma^*) \sim (W^2)^{0.08}$) than at large Q^2 : as a first guess, therefore, one expects that the “true“ (as opposed to: perturbative) QCD-behavior in the infrared region will tend to lower the increase with the energy. Consequently, in our cross section formula (4.1) for the diffractive dissociation we expect that at $t = 0$ the effective power of s/M^2 will be smaller than predicted by our perturbative analysis. How this combines with the t -dependence obtained in our analytic analysis has to be studied in a numerical analysis

which will be the next step in our program.

A last remark should be made on the Pomeron structure function. Although the terminology ‘Pomeron structure function’ is questionable since factorization does not hold in the usual sense, we will nevertheless use it here, since in the literature diffractive dissociation is fairly often discussed in those terms. One of the new elements included into our analysis is the four gluon state in the upper t-channel. Since the two lower Pomerons already come with two gluons each, this four gluon state comes for free, i.e. it costs now extra power of α_s to create this state. In this sense the appearance of the four gluon state in the Pomeron structure function is not as much a higher order effect as in F_2 . One also should bear in mind that, within the BFKL approximation, the four gluon state not only contributes to twist four but also to the leading twist. As to the question under which circumstances this four gluon state contributes, we distinguish between the two cases mentioned before (low mass and high mass). In the former case we have GLAP-dynamics above the triple Pomeron vertex, i.e. the Q^2 evolution is described by the usual (leading twist) evolution equations. The four gluon state only appears in the initial distribution. For the latter case, the upper part is governed by BFKL-type diffusion, and we have seen that the four gluon state may even dominate the two-gluon ladders. Here the Q^2 - evolution will feel the presence of the four gluon state (to describe this in more detail requires a better understanding of the dynamics of the four gluon state). In summary, in the large-mass region we expect the Pomeron structure function to be more effected by the new four gluon state (“screening”) than F_2 , the total deep inelastic cross section.

Acknowledgements: We gratefully acknowledge valuable discussions with M.Ryskin. One of us (J.B.) wishes to thank Al Mueller for very useful conversations.

References

- [1] A.H.Mueller and B.Patel, Nucl.Phys. B 425 (1994) 471
- [2] J.Bartels and M.Wüsthoff, DESY-94-016 (to appear in Z.Phys. C)

- [3] E.A.Kuraev and L.N.Lipatov,V.S.Fadin, Sov.Phys.JETP 44 (1976) 443, Sov.Phys.JETP 45 (1977) 199,
Y.Y.Balitskii and L.N.Lipatov, Sov.J.Nucl.Phys 28 (1978) 822
- [4] ZEUS Collaboration (M.Derrick, et al.), Phys.Lett. B 315 (1993)
- [5] H1 Collaboration (T. Ahmed, et al.), DESY-94-133 (1994)
- [6] L.V.Gribov, E.M.Levin, M.G.Ryskin, Phys.Rep. 100 (1983) 1; E.M.Levin, M.G.Ryskin, Phys.Rep. 189 (1990) 267.
- [7] M.G.Ryskin and M.Besancon, proceedings of the workshop 'Physics at HERA', vol. 1, edited by W.Buchmüller and G.Ingelman (1991) p.215;
E.M.Levin, M.Wüsthoff, Phys.Rev.D 50 (1994), 4306.
- [8] A.H.Mueller, CU-TP-640
- [9] ZEUS Collaboration (M.Derrick, et al.), Phys.Lett. B 332 (1994) 228
- [10] J.Bartels and H.Lotter, Phys.Lett. B 309 (1993) 400
- [11] J.Bartels, M.Vogt, DESY preprint in preparation.
- [12] A.H.Mueller, Nucl.Phys. B 335 (1990) 115
- [13] N.N.Nikolaev and Zakharov, Z.Phys. C 53 (1992) 331
- [14] L.N.Lipatov, Sov.Phys.JETP 63(1986) 904
- [15] A.H.Mueller and W.K.Tang, Phys.Lett. B 284 (1992) 123
- [16] A.M.Polyakov, JETP Lett. 12(1970) 381
- [17] S.Ferrara, R.Gatto, A.F.Grillo and G.Parisi, Nucl.Phys. B 49 (1972) 77
- [18] J.Bartels, Phys.Lett. B 298 (1993) 204, Z.Phys. C 62 (1994) 425

- [19] E.M.Levin, M.G.Ryskin, A.G.Shuvaev, Nucl.Phys. B 387 (1992) 589.
- [20] E.M.Levin, M.G.Ryskin, Sov.Journ.Nucl.Phys. 34 (1981) 619.
- [21] J.R.Forshaw, M.G.Ryskin, DESY-94-162
- [22] J.Bartels, J.R.Forshaw, L.N.Lipatov, H.Lotter, M.R.Ryskin, M.Wüsthoff, DESY-94-244

Figure captions

Fig. 1a : General structure of the cross section of the diffractive dissociation of a virtual photon into $q\bar{q} + n$ gluons in the triple regge limit. Here and in the following figures wavy lines denote reggeized gluons, a shaded circle represents the BFKL-pomeron (eq.2.6), a shaded ellipse represents the pomerons coupling to the proton (eq.2.16) and black ellipses represent different types of $2 \rightarrow n$ gluon interactions.

Fig. 1b : A disconnected contribution to the cross of $\gamma^* + p \rightarrow p + q\bar{q} + n$ gluons.

Fig. 2a : Amplitude of the production of a $q\bar{q}$ - pair in deep inelastic diffractive photon-proton scattering. The summation runs over all different couplings of the two reggeized gluons to the $q\bar{q}$ - pair.

Fig. 2b : Graphical representation of the building blocks of the partial wave amplitude (eq.2.17) of diffractive $q\bar{q}$ - production.

Fig. 3 : Graphical representation of the total cross section $\sigma(\gamma^* + \text{proton})$ (eq.(2.30).

Fig. 4 : A contribution to the amplitude of production of $q\bar{q} + n$ gluons in deep inelastic diffractive photon-proton scattering.

Fig. 5 : Integration path and singularity of the μ - integration (eq.4.2) in the complex μ - plane.

Fig. 6a : Reordering of two-gluon interactions in the four gluon state.

Fig. 6b : Graphical representation of the effective vertex (eq.4.34) for the recoupling from interaction channels $(ij),(kl)$ to $(ik),(jl)$.

Fig. 6c : Compact representation of the four gluon state as a state of two pomerons interacting via an effective recoupling vertex.

Fig. 7 : The contribution (4.38) to the cross section of diffractive production of $q\bar{q}$ + gluons with a single pomeron interaction in the four gluon state.

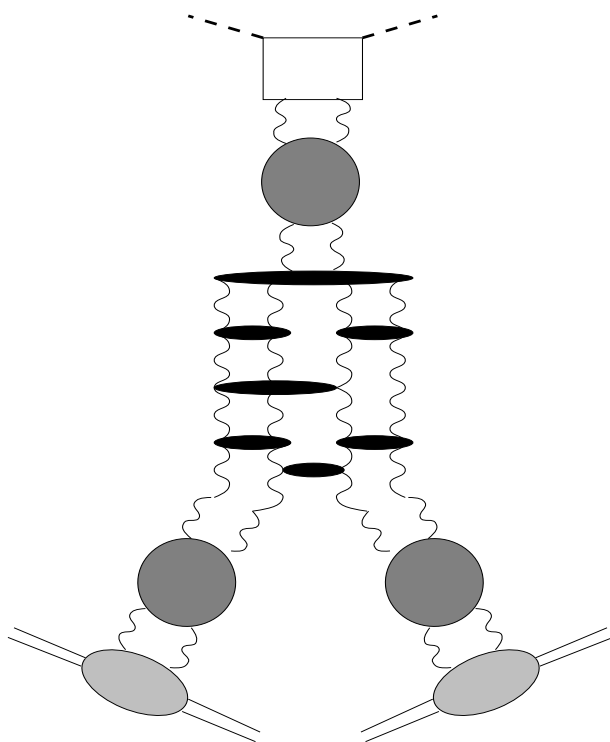


Figure 1a:

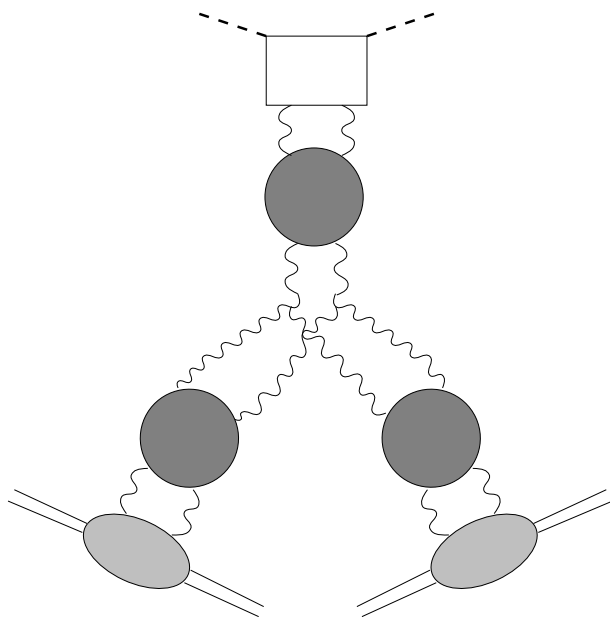


Figure 1b:

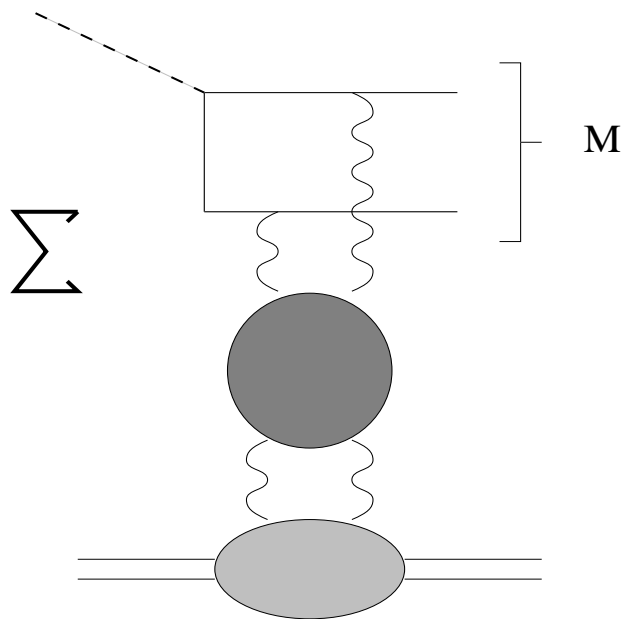


Figure 2a:

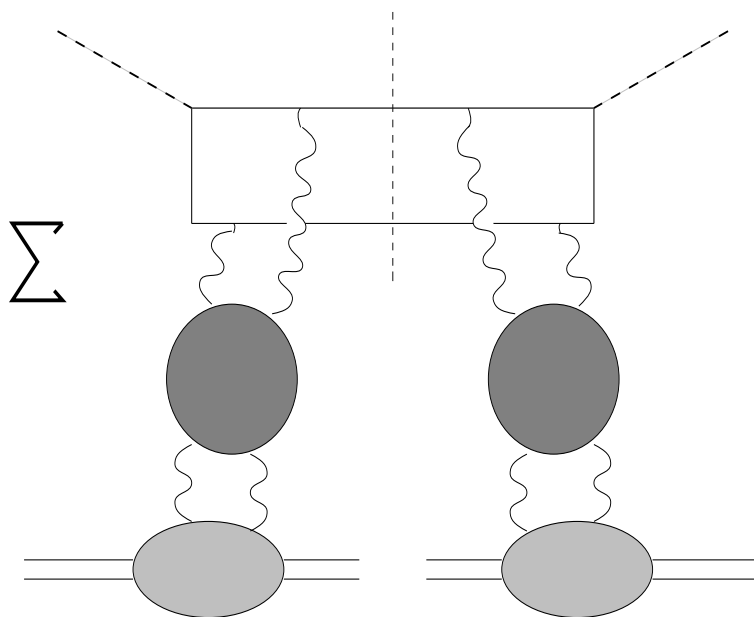


Figure 2b:

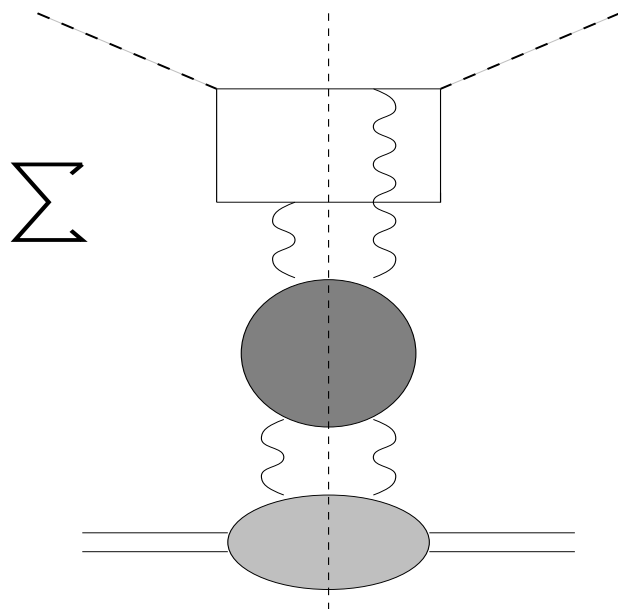


Figure 3:

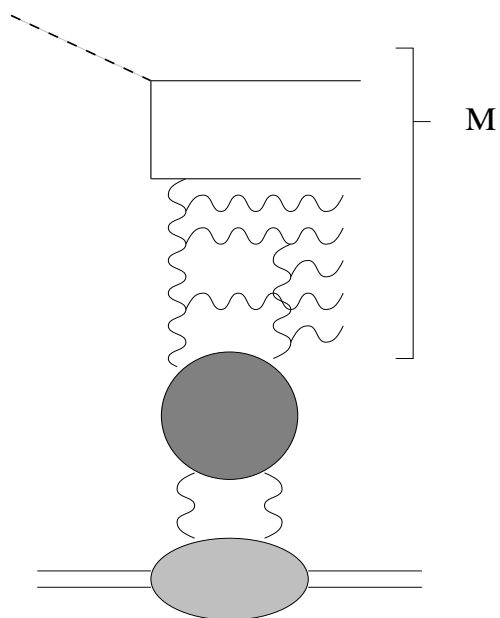


Figure 4:

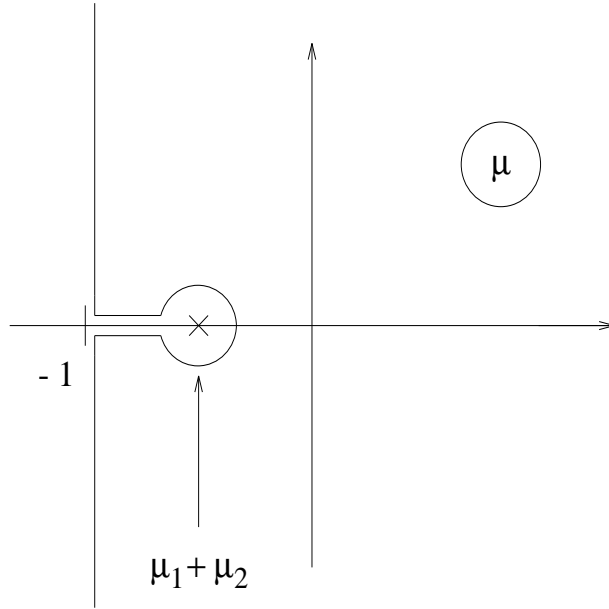


Figure 5:

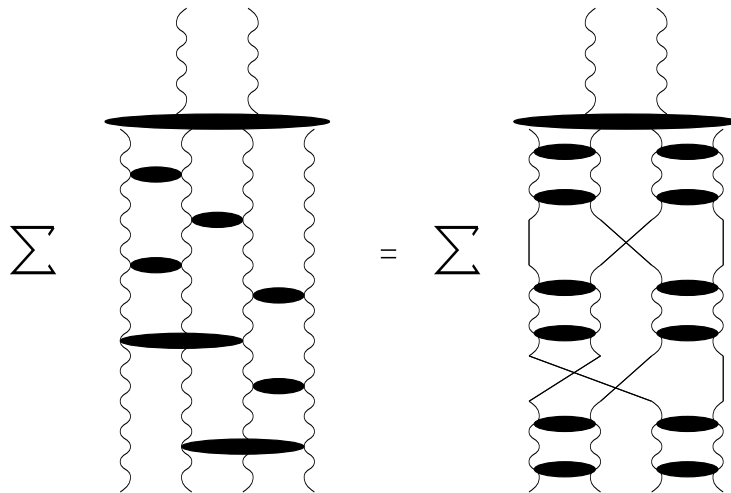


Figure 6a:

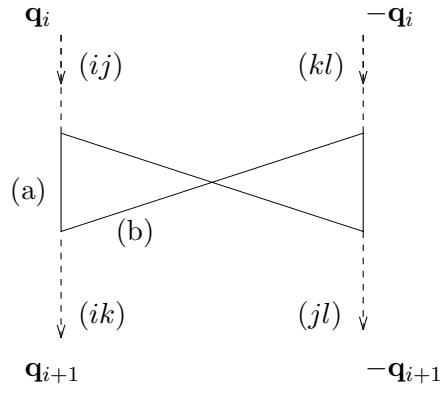


Figure 6b:

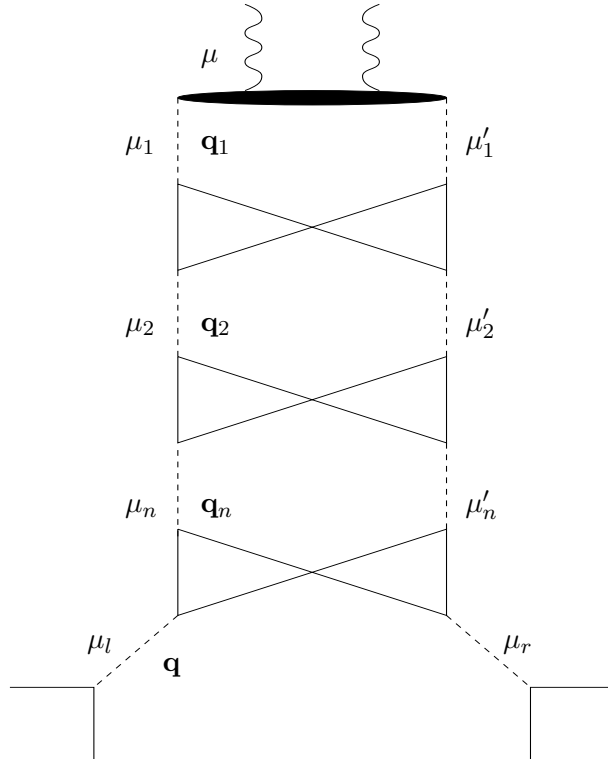


Figure 6c:

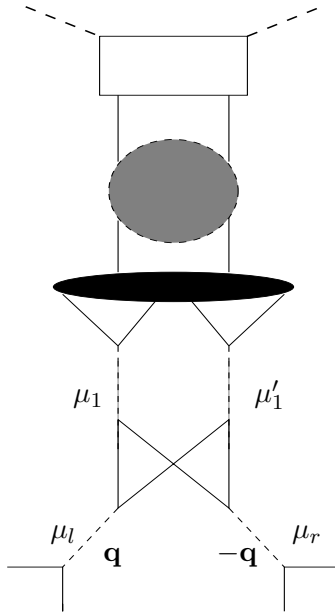


Figure 7: